Astron. Astrophys. 328, 290–310 (1997)

ASTRONOMY AND ASTROPHYSICS

The remarkable asymmetric outflow from the Cygnus Egg Nebula

C.J. Skinner[1,2,3], M. Meixner[4,5,12], M.J. Barlow[6], A.J. Collison[7], K. Justtanont[8], P. Blanco[9], R. Piña[9], J.R. Ball[3,10,12], E. Keto[11,12], J.F. Arens[10], and J.G. Jernigan[10]

[1] Space Telescope Science Institute, 3700 San Martin Drive, Baltimore, MD 21218, USA;
on assignment from the Space Sciences Department of the European Space Agency
(email: skinner@stsci.edu)
[2] Laboratory for Experimental Astrophysics, Lawrence Livermore National Laboratory
[3] Institute of Geophysics & Planetary Physics, Lawrence Livermore National Laboratory
[4] Department of Astronomy, University of California, Berkeley
[5] Department of Astronomy, MC221, 1002 W. Green Street, University of Illinois, Urbana, Il 61801, USA
[6] Department of Physics & Astronomy, University College London, Gower Street, London WC1E 6BT, UK
[7] Department of Physics, Loomis Laboratory, 1110 W. Green Street, University of Illinois, Urbana, Il 61801, USA
[8] NASA-Ames Research Center, MS245-3, Moffett Field, CA 94035, USA
[9] Center for Astrophysics & Space Science, Code 0111, University of California San Diego, La Jolla, CA 92093-0111, USA
[10] Space Sciences Laboratory, University of California, Berkeley, CA 94720, USA
[11] Lawrence Livermore National Laboratory, L-59, P.O.Box 808, Livermore, CA 94551-9900, USA
[12] Visiting astronomer, NASA Infrared Telescope Facility.

Received 11 August 1996 / Accepted 20 May 1997

Abstract. We present ground based continuum images in the infrared, from 1.2 to 19μm, and an H_2 2.122μm line emission image of the post-AGB star AFGL2688, the Cygnus Egg Nebula. We show that the standard model of this source, comprising a fast wind focussed by a dense, equatorial, dusty torus into a bipolar flow at position angle 15° and close to the plane of the sky, cannot explain the combination of kinematic information from previous studies and morphological information in our own observations. Nor are the images consistent with a classical bipolar flow, since the apex of the two lobes observed in scattered light in the visible and near-IR are offset in R.A. with respect to one another. We suggest a model which is physically similar, but substantially different geometrically, in which there is a bipolar flow at a position angle closer to 60°, rather than 15°, still collimated by a dense, equatorial, dusty torus, but the opening angle of the cones out of which the fast bipolar flow is directed is closer to 90°, rather than 20° or so as previously suggested. The bipolar flow axis is inclined by about 20–30°, rather than in the plane of the sky as in previous models. The dust distribution in the nebula has to be extremely clumpy, and there is evidence that large scale mass loss from the progenitor AGB star occurred in discrete phases, recurring on a timescale of ∼750 years. This model implies a much lower velocity for the 'fast' bipolar outflow than does the standard model, which is consistent with very recent Nobeyama Millimetre Array images in ^{13}CO emission. In support of our new model, we present a full radiative transfer model for the source, in axial symmetry, which reveals that the final phase of heavy mass loss included a superwind phase which lasted about two hundred years and removed about 0.7 $M_\odot$ from the envelope of the progenitor AGB star. Our results imply that the progenitor star must have been a relatively high mass AGB star. Our radiative transfer model also demonstrates convincingly that, in contrast with previous models, the core of the nebula has to be exceptionally optically thick, with an optical depth greater than unity even at 10μm.

Key words: circumstellar matter – stars: evolution – stars: individual (AFGL2688) – stars: AGB and post-AGB – stars: mass-loss – infrared: stars

1. Introduction

Stars at the tip of the AGB lose mass copiously in the form of slow and dense stellar winds. Dust in the winds reddens the central starlight, and in many cases renders the star optically very faint or invisible (e.g. IRC+10216, OH26.5+0.6). The energy distribution of such extreme AGB stars typically peaks in the mid-IR, by virtue of the thermal reradiation by the optically thick circumstellar dust shells. In contrast, planetary nebulae (PN), which are the evolutionary descendants of the AGB stars, show little circumstellar reddening, and have spectral energy distributions which peak in the mid- or far-IR (e.g. NGC7027).

By implication, objects in transition between the AGB star and PN phases of their evolution should simultaneously exhibit

Send offprint requests to: C.J. Skinner

rising stellar effective temperatures, and dust excesses which move to longer wavelengths as the dust shells coast outwards and cool, along with decreasing circumstellar reddening. Such transition objects are often referred to as protoplanetary nebulae, since it is assumed that they will evolve into PN. However, the speed with which such objects evolve is not yet observationally established, hence it is not actually certain that all such objects will become PN. We therefore refer to them as post-AGB stars.

One of the first such transition objects to be discovered was AFGL2688, noted by Ney et al. (1975) because of its extreme brightness in the mid-IR and very cool colours (∼200K), and discovered by them to be associated with a spectacular bipolar optical reflection nebula, consisting of two tulip shaped lobes on an axis at a position angle of about 15°. A pair of horns is seen projecting out from each lobe away from the center of the nebula. It had in fact previously been catalogued as a probable galaxy (IV Zw 67), and is known as the Cygnus Egg Nebula because of its egg-like appearance on the Palomar sky survey plates. Distance estimates to AFGL2688 have generally been in the range 1.0 to 1.5kpc (Crampton, Cowley & Humphreys 1975; Cohen & Kuhi 1977); we will adopt in this work a value of 1.2kpc, intermediate in this range. The central star, obscured by its circumstellar dust shell but observable in the reflection nebulosity, has F5Ia spectral type (Crampton et al. 1975) consistent with a post-AGB status. Anomalous bands due to C_3 and C_2 indicate that AFGL2688 is C-rich, presumably descended from a C-star (Crampton et al. 1975). Single dish molecular line observations of AFGL2688 in the ^{12}CO J=1–0 line show the classical parabolic line profile that suggests an optically thick, spherical shell of molecular gas coasting outwards at a constant velocity, presumably produced by the progenitor AGB star (Knapp & Morris 1985). Truong-Bach et al. (1990) mapped AFGL2688 in the CO J=2-1 and J=1-0 lines, and showed that the AGB wind remnant is spherical. Observations in a number of mm-wave molecular lines by Young et al. (1992) suggested to them that AFGL2688 has at least three velocity components: a dominant, slow, 23km/sec expansion velocity wind due to the AGB progenitor, a 'medium velocity' 45km/sec wind, and a high velocity component with velocities up to ∼100km/sec, with the highest velocity component closest to the star, and the lowest furthest from the star. Evidence for interacting winds preceded these observations: Thronson (1982) observed shock-excited molecular hydrogen lines in the near-IR spectrum of AFGL2688, taken by him to be produced by the interaction of winds with different velocities. This interpretation was strengthened by the observation by Beckwith, Beck & Gatley (1984) that the molecular hydrogen emission was confined to the bipolar lobes. These authors argued that the shocks are generated where a fast bipolar outflow from the warm central star interacts with a slower wind from the progenitor AGB star. Velocity resolved images in the molecular hydrogen S(1) 1–0 line at 2.122μm by Smith et al. (1990) show a most remarkable and unexpected structure: the molecular hydrogen emission is seen in four blobs spaced equally about the central object, two lying in the optical bipolar lobes and two orthogonal to them. The N and E blobs are tipped towards us, and each have LSR velocities of about –60km/sec, whilst the S and W lobes are pointed away from us and each have LSR velocities of about –30km/sec. Latter et al. (1993) interpreted their narrowband images of H_2 2.122μm emission, which also show four blobs, in terms of a model in which the N-S blobs arise from shock excitation in the bipolar lobes where the fast wind punches through the AGB wind remnant, and the E-W blobs arise from shock excitation where the fast wind crashes into a rotating torus observed in HCN J=1-0 line emission by Bieging & Rieu (1988). However, if the H_2 velocities of the E-W blobs are actually rotational, then the rotation rate is unprecedentedly large for an AGB envelope.

In an attempt to investigate the morphology of the inner, most active regions of AFGL2688, we have taken high angular resolution images at infrared wavelengths in the continuum from 1.2 to 19μm, and narrowband images of the 2.12μm H_2 line emission. We present our images of AFGL2688 in the next section. In Sect. 3 we discuss the standard model of the nebula, and the deficiencies which lead us to propose a revised model of the source. We describe this alternative model for the nebula in Sect. 4, and show how it better explains observations of AFGL2688. In Sect. 5, we develop a detailed radiative transfer model for the spectral energy distribution (SED), quantitatively compare the standard model and our new model, and determine the mass loss history of the star in the later stages of its AGB evolution. In Sect. 6, we discuss the results and their implications for the nature of the progenitor of AFGL2688 and for other post-AGB stars.

2. Observations and results

We obtained images of AFGL2688 in a number of observing sessions (see Table 1 for summary). Near-IR images were all obtained with the 3.8m United Kingdom Infrared Telescope[1] using the facility near-IR camera IRCAM, which employed a 62×58 pixel InSb array (McLean et al. 1986). Images were obtained at a pixel scale of 0.62″in the J, H and K bands in June 1990, and in October 1990 in the K band, in the H_2 S(1) 1-0 line at 2.122μm with a 1% spectral bandwidth filter, and at 3.4μm with a 4% bandwidth filter (nbL). During June 1993 images were obtained at 0.62″pixel scale in the J and K bands, at nbL, in the H_2 S(1) 1-0 line and in the continuum at 2.104μm with narrow bandwidth filters, as well as at 0.31″pixel scale in the H_2 S(1) 1-0 line. All observations were taken in stare mode, with stares of various integration times being alternated between source and sky, and a sky frame subtracted from the source frame to remove the sky background emission. The sky frame was used in each case to flat-field the source image. In all cases an integration identical to the source observation was made looking at a cold stop in order to approximately subtract the dark current. Observations of the standard stars BS8143 and HD203856 were used to flux calibrate the images, and to determine the point spread function (psf), which was approximately 1.2″(FWHM) for the images with 0.6″pixels and 0.6″(FWHM) for the image

[1] UKIRT is operated by the Royal Observatory, Edinburgh, on behalf of the UK Science & Engineering Research Council

with 0.3″pixels (since we had fewer than 2 pixels per resolution element, our spatial resolution is limited by the pixel size rather than by the seeing or the telescope performance).

Mid-IR images were made at the NASA Infrared Telescope Facility[2] during May 1991. We used the Berkeley/Livermore Mid-IR Array Camera, which employs a Hughes 10×64 pixel Si:Ga array detector (Arens et al. 1987a, 1987b; Keto et al. 1992). Images at 8.8μm, 10μm, and 11.5μm were made using a ∼10% spectral bandwidth circular variable filter (CVF), and images at 8.2μm and 9.7μm were taken using a ∼ 1.3% spectral bandwidth CVF. In each case a mosaic was assembled out of 3 to 5 10×64 pixel panels in order to cover the extent of the IR nebula. Sky subtraction was achieved by nodding and chopping as described by Ball et al. (1992), and flux calibration was done by comparing observations of the standard star α Her. After each frame was sky subtracted and flat-fielded, any bad pixels were removed by interpolation using IRAF. The frames were then assembled automatically into a mosaic using a program which minimises the variance between frames in the overlap regions (Meixner 1993). The point source calibrator α Her was used to determine the psf, which was found to be approximately circular, with FWHM ∼1.5″: this is considerably worse than the diffraction limit for this telescope, and rather worse than we have experienced on other observing runs at the IRTF.

An image was obtained at a wavelength of 19.2μm at the 60-inch IR telescope on Mt. Lemmon, using the UCSD/Minnesota mid-IR camera (Piña 1994). These data were sky subtracted, flat fielded and flux calibrated in a similar fashion to the IRTF images. Careful comparison of this image with a variety of point source calibrators taken through the night indicated that AFGL2688 was basically unresolved at this wavelength, and that the source size is less than 2″(FWHM).

Image reduction for the near-IR and mid-IR images was done partly in Starlink's IRCAM package and partly using IRAF[3]. The 19.2μm image was reduced using tasks developed in the IDL software package. Further details of those images presented here are listed in Table 1.

The 1993 J-band image is shown in Fig. 1. Both of our broadband K images show the same structure and details as Fig. 4c in Latter et al. (1993), namely N-S lobes similar to the optical nebula, plus a pair of E-W "ears." We do not present these, nor the H-band image, which is identical to Fig. 4b of Latter et al. (1993), and very similar to our J-band image, because they add little to the discussion in this paper, and because the broadband K images contain a complex mix of continuum and H_2 emission, whereas our 2.104μm narrowband image contains only continuum flux, with no contribution from any lines (Hora & Latter 1994), and so is more informative. For broadband H or K images, the interested reader is encouraged to consult Latter et al. (1993). The narrowband L image (3.4μm, nbL) in Fig. 2 shows

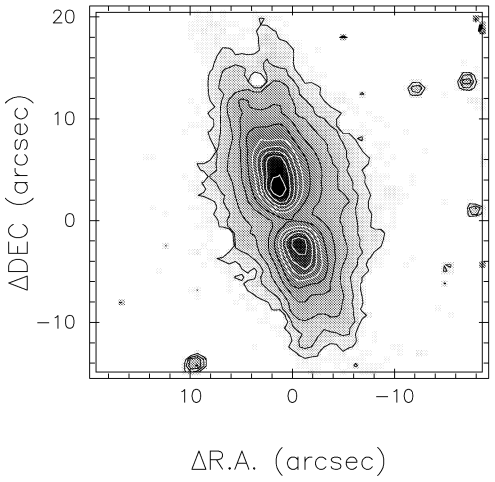

Fig. 1. UKIRT J-band image of AFGL2688, presented in grey-scale with contour overlay. The grey scale and the contours are logarithmic, pixel scale is 0.62″. The upper contour is 2.1mJy/arcsec^2 and the lower contour 2.1μJy/arcsec^2.

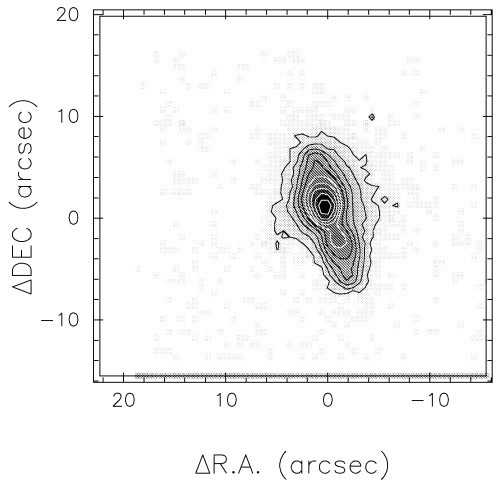

Fig. 2. Narrowband L (nbL) image of AFGL2688, presented as Fig. 1. Upper contour 117mJy/arcsec^2, lower 0.29mJy/arcsec^2.

the N-S lobes almost joined together, giving the appearance that the Egg contains a tadpole (unusual offspring for Cygnus, the Swan). The three mid-IR images at wavelengths of 8.8μm, 10.0μm and 11.5μm, appear more or less identical (only one is shown in Fig. 3). The other two images (8.2 and 9.7μm) have significantly lower S/N, due to the smaller bandwidth of the observations, and do not show any further detail. Despite the rather worse than usual spatial resolution, our mid-IR images are consistent with those presented by Hora et al. (1995), which were taken at UKIRT in 1993.

While there are clear differences between the images at different wavelengths, there are a number of morphological features in common. At the lowest flux levels, there is a hint of a rectangular structure in all the images where the vertices are the prominent N-S lobes and the fainter E-W lobes seen more prominently at longer wavelengths. The rectangular structure

[2] The NASA IRTF is operated by the University of Hawaii under contract with the National Aeronautics and Space Administration

[3] The Image Reduction and Analysis Facility is distributed by the National Optical Astronomy Observatories, which is operated by the Association of Universitiies for Research in Astronomy, Inc., under contract to the National Science Foundation.

Table 1. Observation details

Wavelength (μm)	Bandpass	Integration time per pixel (sec)	Pixel scale (arcsec)	Date	Telescope
1.2	J-band	4500	0.62	19/09/1993	UKIRT
2.104	1%	600	0.62	15/06/1993	UKIRT
2.122	1% (H_2 S(1) 1-0)	2100	0.62	15/06/1993	UKIRT
2.122	1% (H_2 S(1) 1-0)	2100	0.31	20/06/1993	UKIRT
3.4	4% (nbL)	960	0.62	23/06/1993	UKIRT
8.8	10%	21	0.39	14/05/1991	IRTF
10.0	10%	21	0.39	13/05/1991	IRTF
11.5	10%	32	0.39	13/05/1991	IRTF
19.2	10%	1000	0.82	31/10/1993	Mt. Lemmon 60″

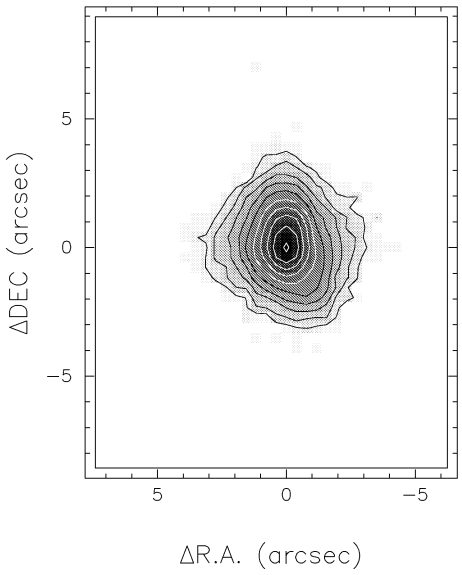

Fig. 3. IRTF mid-IR image of AFGL2688, taken with a 10% bandwidth CVF, centred on a wavelength of 8.8μm again presented as Fig. 1. Pixel scale is 0.39″. Upper contour 39Jy/arcsec^2, lower 0.39Jy/arcsec^2.

dominates the mid-IR images. The rectangle is largest in the J-band image, and smallest in the mid-IR and the horns which are so striking at I (Latter et al., 1993) and at J become progressively less apparent with longer wavelengths, consistent with the decrease in scattering efficiency of the dust and increase in thermal emission as the wavelength is increased. In all the near-IR images, there is a significant E-W asymmetry in the nebula, the emission appearing more extended to the western edge of the center than to the eastern edge. At the higher flux levels, the N lobe appears to orient almost due N, whilst the S lobe appears skewed significantly W of S. As we move to longer wavelengths, the angular separation of the N and S lobes decreases with increasing wavelength and the western skew of the S lobe with respect to the N lobe becomes more apparent. At mid-IR wavelengths the N-S lobes are joined together and are clearly skewed in angle.

The 1993 H_2 S(1) 1-0 images are presented in Figs. 4a (0.62″/pixel) and 4c (0.31″/pixel). The "ears" seen in broadband K images are seen clearly in Fig. 4c. The 2.104μm continuum image is presented in Fig. 4b, and we now see that, with reasonable S/N, part of this E and W blob structure is visible in scattered continuum as well as in the line emission. With a larger field of view, in Fig. 4a, we see two additional features – two very faint blobs on an axis through the center of the nebula at position angle ∼75°, and at about 11″from the center of the nebula. There is a finite chance that these two blobs are ghosts because we did collect some ghost images in some of the narrowband observations during these observing runs; however, we made checks using single standard stars and all these checks failed to produce any pairs of ghosts consistent with these two features, at this or any other wavelength.

The 2.122μm image presented in Fig. 4a contains a large contribution from scattered continuum emission. We have subtracted the 2.104μm continuum image from the 2.122μm image to yield a nearly pure H_2 image which we present in Fig. 5. Uncertainties in the flux calibration[4] of the original images presented here will impart some errors into Fig. 5, and so the precise details of the structure revealed in Fig. 5 must be treated with some caution. However, the gross morphology should be correct. Given the S/N of the various observations, Fig. 5 herein agrees with the H_2 observations of AFGL2688 in Beckwith, Beck & Gatley (1984) and Smith et al. (1990), but is of considerably higher S/N and so reveals fainter structure than any previous images at this wavelength.

In molecular hydrogen the nebula is spectacular. The molecular hydrogen emission is more than just photogenic; it is very revealing. The E-W structure ascribed by Latter et al. to a torus is highly clumped, indicating that the nebula as a whole probably has a very inhomogeneous structure. The filaments linking the N and E blobs and their radial velocities (Smith et al. 1990) very strongly suggest that there is a physical link between these two blobs. A fainter but significant filament also connects the S and W H_2 blobs suggesting a physical link for this pair as well. The two new H_2 blobs at PA 70° and the elongation of the mid-IR images delineate yet another axis through the middle of the

[4] Images in the H_2 line are usually calibrated using observations of standard stars, which contain only continuum emission within the spectral bandpass of the filter; since the transmission of the filter will vary strongly with wavelength, such calibrations are in general not very accurate. A better practise would be to use H_2 line emission sources of well known line flux.

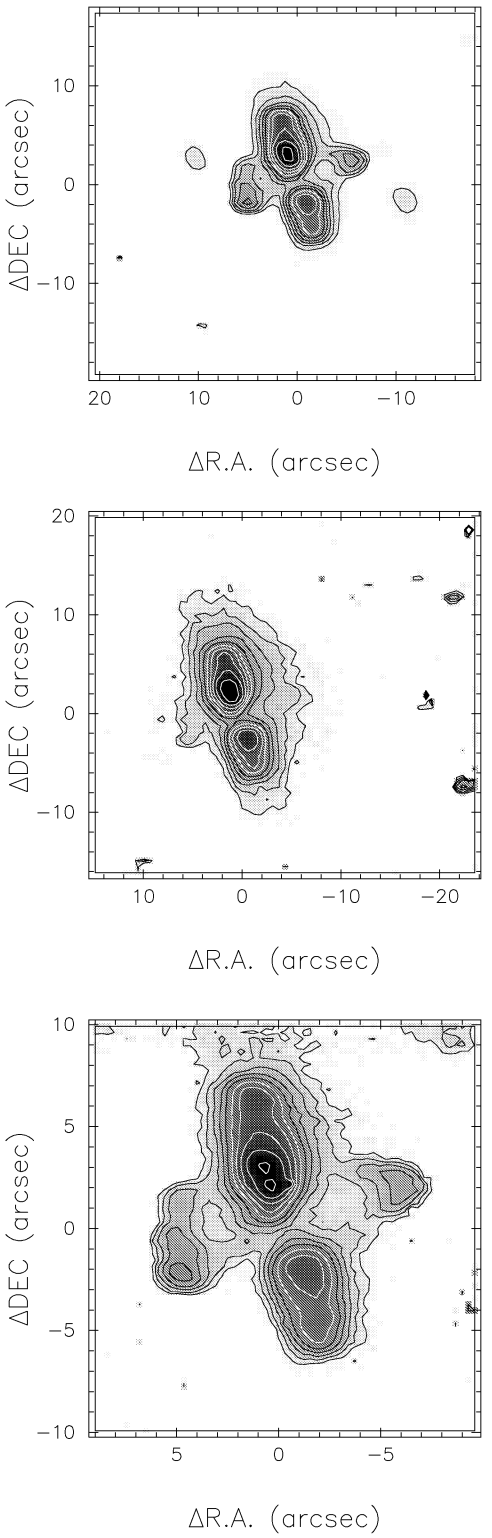

Fig. 4. Narrowband images in the 2μm region of AFGL2688 from UKIRT, presented as Fig. 1. From top to bottom: **a** 2.122μm image, upper contour 4.4mJy/arcsec^2, lower 34μJy/arcsec^2. **b** 2.104μm image, upper contour 20mJy/arcsec^2, lower 44μJy/arcsec^2. **c** 2.122μm image at 0.31″/pixel, upper contour 4.1mJy/arcsec^2, lower 41μJy/arcsec^2.

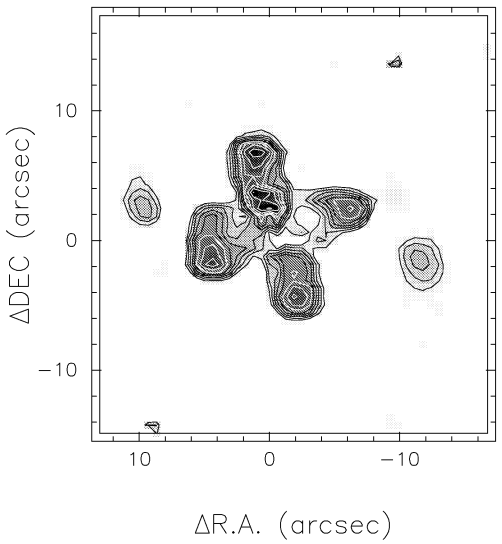

Fig. 5. Difference between Figs. 4a and 4b, which represents the pure molecular hydrogen emission, presented as Fig. 1 again. Upper contour 390μJy/arcsec^2, lower 12μJy/arcsec^2.

nebula. The two detached H_2 blobs or ansae are highly reminiscent of the ansae and FLIERs (Fast Low-Ionization Emission Regions; Balick et al. 1993a,b) that appear in about 20% of the sample of bright and moderately compact planetary nebulae imaged by Balick (1987). These features possess high velocities relative to the surrounding nebular gas and usually have smaller dynamical ages. The possibility that bow-shock excitation is responsible for many of the observed characteristics of PN FLIERS was considered by Balick et al. It would be of some interest to determine the velocities of the detached H2 ansae in AFGL2688 to see if they too are moving at high velocities.

In Fig. 6 we present a dust temperature map generated from the ratio of 11.5μm to 8.8μm emission. Before making far-reaching conclusions from this map, we point out that the interpretation, and even the validity, of such a map must be questionable in such a nebula. Temperature and optical depth maps can be derived for observations of optically thin nebulae, under the assumption that the optical depths at the two wavelengths are very similar at each position, and that the nebular temperature is very similar at the two wavelengths. In the case of an extended, optically thick nebula, the radiation from below the unit optical depth surface is largely lost, and the temperature at a given position is largely determined by the depth to which we can see. Deutsch (1990) assumed an optically thin nebula and derived, for the center of the AFGL2688 nebula, an optical depth at 9.8μm (0.037) larger than that at 8.3μm (0.013), which appears inconsistent with properties of the amorphous carbon grains that are believed to comprise the majority of the grains in the Egg nebula and that have a larger opacity at 8.3μm than at 9.8μm. In the model which we present in Sect. 5, the dust nebula is optically thick and the temperature in the inner region changes very rapidly with depth. Because we see to somewhat different depths at 8.8 and 11.5 μm, the intensity ratio maps will no longer

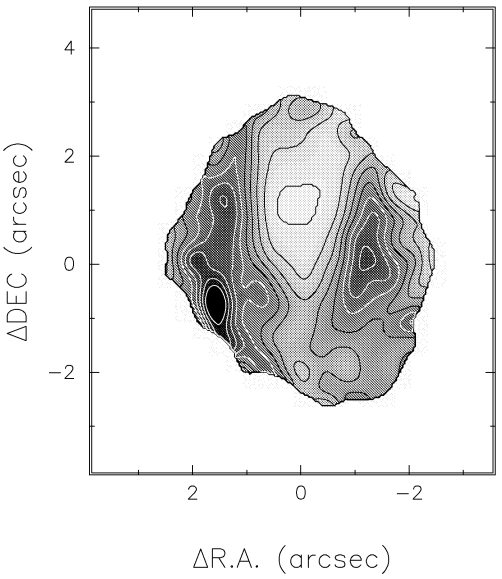

Fig. 6. Dust temperature map made using the 8.8 and 11.5μm images. Temperatures are contoured linearly from 120K to 172K. Note that these temperatures may be misleading, as explained in the text.

fulfil the assumptions used in deriving temperatures and optical depths. Thus one must be extremely cautious in interpreting Fig. 6. Nevertheless, we find that the derived temperatures range from 120K to 170K, which is a reasonable range, consistent with the range of temperatures predicted by the model in Sect. 5. The morphology of the temperature map is ambiguous. One could interpret the E and W minima as being consistent with the presence of a strongly absorbing torus, whose plane lies on the line connecting the E and W minima (Sect. 3), as predicted by the standard model. However, our alternative model (Sect. 4) also predicts temperature minima behind the material that is shadowing part of the lobes. Hence, this temperature map could be taken to be consistent with either model.

3. The standard model For the AFGL2688 nebula

From the very extensive observational database available, a fairly detailed model for AFGL2688 has evolved, which is discussed in some detail by Latter et al. (1993), for example. According to this "standard model", the progenitor C-star left the AGB a few hundred years ago, at which time the star had a very massive, and equatorially concentrated wind. This generated a dense equatorial torus of dust, which currently totally obscures the central star. Visible and near-IR radiation from the central F5Ia star escapes along the polar axes and is scattered off dust, forming the spectacular bipolar reflection nebula. The current fast wind from the warm central star is focussed along the polar axes by the dense equatorial torus, generating a very fast bipolar flow, which punches its way through the surrounding, more or less spherical and slower AGB wind. The axis of the bipolar flow lies at position angle 15°, and is inclined at about 5–15° to the plane of the sky. Despite its wide acceptence, we find that there are a number of observations that the standard model fails to explain, and we outline these in this section. In the next section we will propose an alternative model which we suggest accounts better for AFGL2688's observational properties.

Foremost is the velocity structure revealed by the H_2 images of Smith et al. (1990). The bipolar flow is supposed to be aligned roughly N-S, yet the N and E H_2 blobs have the same velocity to within a few km/sec, as do the W and S blobs. The velocity difference between the two pairs (N-E and S-W) of blobs is of order 30km/sec. Latter et al. ascribed the velocities of the E and W blobs to the rotation of the torus claimed by Bieging & Rieu (1988). However, the rotation velocity 4″E and 4″W of the central object in Bieging & Rieu's data is only ∼1km/sec, an order of magnitude too small. Additionally it is exceedingly unlikely that the projected velocities of the N and S bipolar lobes would coincidentally be identical to those of the E and W limbs of the rotating torus. It is much more likely that the N and E blobs are physically related to one another, and likewise the S and W blobs.

Second, Young et al. (1992) reported velocities up to ∼100km/sec in the outflow from AFGL2688. If the bipolar axis is inclined at ∼15° to the plane of the sky, then the bipolar flow velocity, by the arguments presented by Young et al., is ∼350km/sec. If the inclination angle is close to 5°, as required by the "standard model" (e.g. Latter et al. 1993), then the bipolar flow speed is ∼1000km/sec. This velocity is extraordinarily high. The similar, and possibly related, C-rich bipolar nebula GL618 has a high velocity wind component with velocities reaching no more than ∼270km/sec (Cernicharo et al., 1989, assuming an inclination angle for the AFGL618 nebula of 45°), despite having a hotter central star and more highly excited bipolar nebula. Another evolved star, OH231.8+4.2, has a bipolar outflow with a velocity of ∼ 140 km/sec (Morris et al. 1987, assuming an inclination angle for the OH231.8+4.2 nebula of 47°). No known post-AGB star or PN exhibits an outflow with so high a veolcity. However, if the bipolar axis of AFGL2688 were inclined at a much larger angle to the plane of the sky than 5°, the deprojected bipolar flow speed becomes much smaller, and comparable to those of other nebulae.

Third, whilst Latter et al. suggest the E-W structure seen in their broadband K image is an equatorial torus, close examination of the observed K-band morphology reveals an inconsistency and suggests another possibility. If the bipolar axis is really inclined at an angle of 15° to the sky, and the equatorial torus lies in a plane orthogonal to the bipolar axis, as expected in the standard model, then the ratio of the semi-major to semi-minor diameters of the projected torus should be ∼3.9. If the inclination angle is actually 5°, as Latter et al.'s model suggests, then the ratio should be ∼11.5. The ratio we measure from the K image of Latter et al. is ∼2 demonstrating that the standard model is not consistent with the observations We have already mentioned the filaments which appear to link the N to E blobs and the W to S blobs, and we will suggest in the next section that these pairs of blobs are really physically connected, each a part of a single structure much larger than the individual blobs.

Fourth, the torus of H_2 emission proposed in the standard model has an implausibly large radius of ∼5″(∼10^{17}cm at 1.2

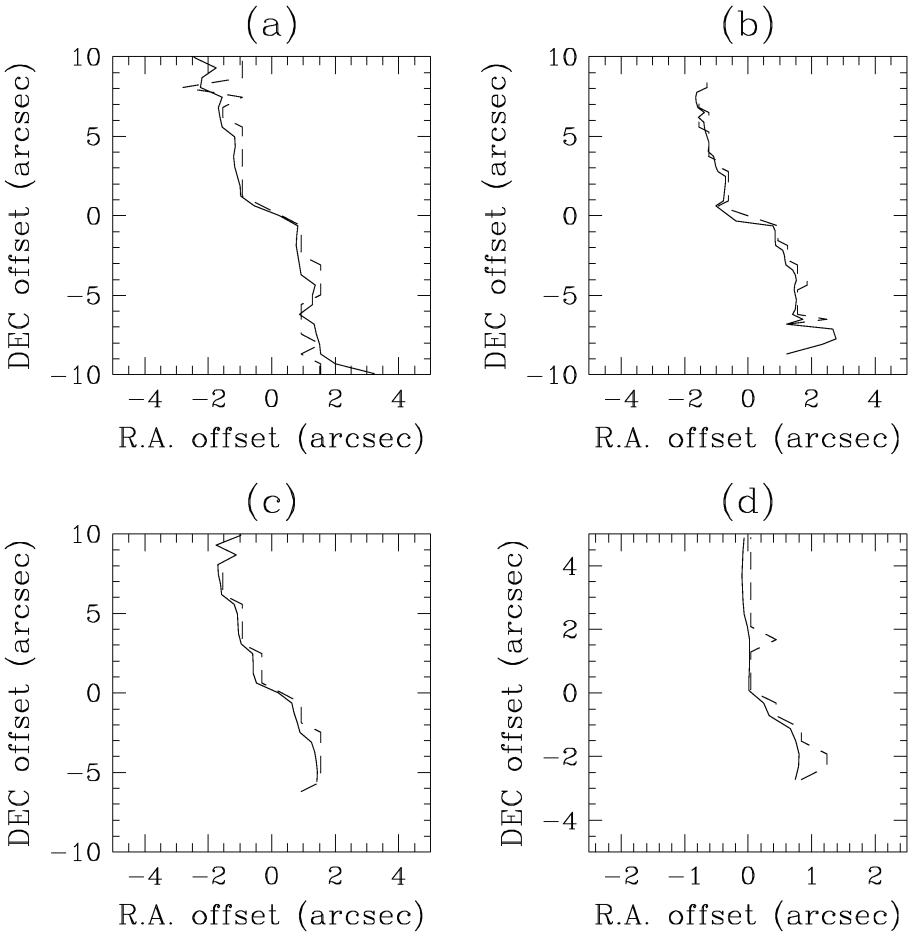

Fig. 7. Plots of the R.A. flux averaged center of brightness (solid line; see text for definition) of the nebula against DEC. and the R.A. position of the brightest point (dashed line) against DEC., for **a** the J-band image, **b** the 2.122μm (0.31″/pixel) image, **c** the nbL image and **d** the 11.5μm image.

kpc), which is inconsistent with other observations, and suggests a dynamical structure for the nebula that is unstable. If we believe the well substantiated suggestion that the H_2 emission of the torus arises from the shock excited gas of the colliding fast post-AGB wind and slow AGB wind, then we would expect this excitation on the inner edge of the torus. However, all models of AFGL2688's emission strongly suggest an inner radius of $\sim$1″or less (e.g. Latter et al. 1993; Jura& Kroto 1990; this work), at least five times smaller than the observed H_2 radius. If one maintains that the E-W H_2 emission regions are the outer edges of a very large torus that is rotating at the 15 km/s velocity measured by Smith et al. (1990) then we find inconsistencies with other observations. According to the mm-wave observations of AFGL2688 by Truong-Bach et al. (1990) the circumstellar envelope is approximately spherically symmetric with a FWHM of $\sim$16″(resolution of $\sim$6″). Bieging & Rieu (1988) imaged AFGL2688 in the HCN line at 5″resolution and found a moderately flattened structure rotating at 1.2 km/s aligned with the dust lane; however, the angular resolution of those observations is insufficient to clearly resolve a toroidal structure leaving the interpretation of a torus uncertain. If the rotation is a result of mass loss induced by binary interaction, the angular momentum in Bieging & Rieu's torus rotating at 1.2km/sec is already implausibly large (they indicate that it is about two orders of magnitude larger than could be sustained by any binary system with components in the mass-range of AGB star progenitors): Latter et al.'s suggested 15km/sec rotation velocity and larger radius makes the problem almost two orders of magnitude worse. Neither can the toroidal rotation be induced by magnetic corotation of the wind and central star. If we follow the argument presented by Bieging & Rieu (1988), the stellar magnetic field strength necessary to generate a 15km/sec rotation velocity at $\sim 10^{17}$cm is 10^6G. There is no known way to sustain a torus of such dimensions rotating so rapidly. Additionally, a structure of this size rotating so rapidly should have been strikingly obvious in the observations by Bieging & Rieu (1988) or Truong-Bach et al. (1990). To explain the kinematics of the AFGL2688 nebula, we require some explanation other than a rotating torus.

Fifth, the scattering models presented by Latter et al. (1993) and Yusef-Zadeh, Morris & White (1984) for AFGL2688 differ with the data in two important ways, noted by Latter et al. (1993). First, at all wavelengths the model's intensity gradient outward along the bipolar lobes rises too steeply at the inner edges of the scattering lobes in the models when compared with the observed images. Second, as the wavelength increases, from I to K, the lobe intensity peaks of the AFGL2688 images move spatially closer together, while in the models of Latter et al. (1993) the intensity peaks remain almost fixed in position. Latter et al. (1993) suggest that the differences between the observations and the model arises because they used only single

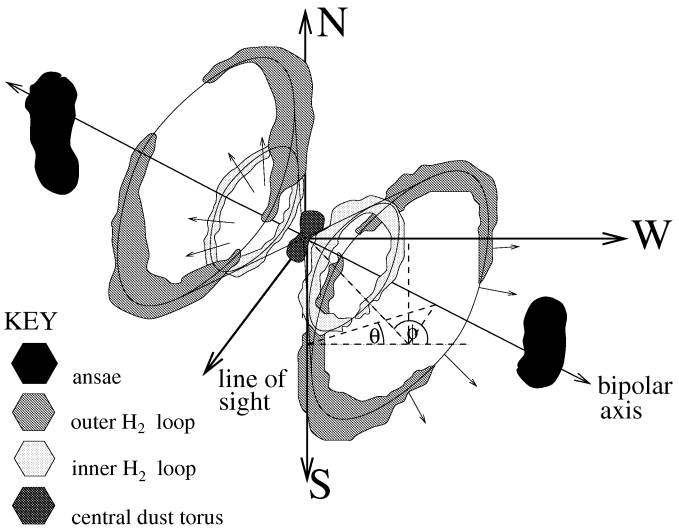

Fig. 8. A schematic view of our new model highlighting the location of the main features of the AFGL2688 nebula. The inclination of the bipolar axis to the plane of the sky (θ) and the P.A. of the bipolar axis (ϕ) are indicated. For further description see text.

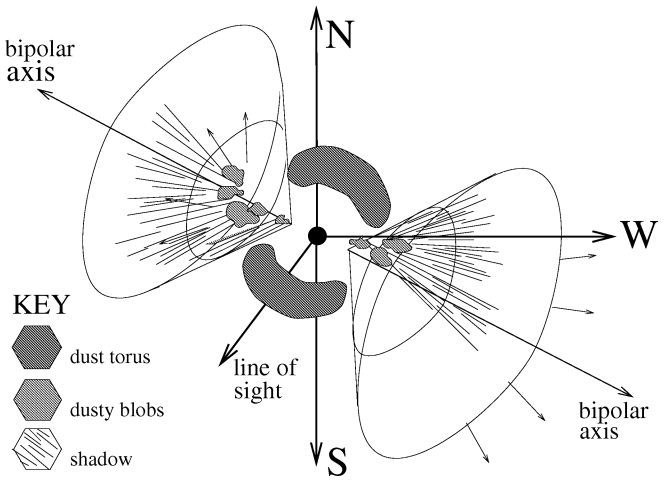

Fig. 9. A schematic view of the AFGL2688 nebula, in which dusty blobs in the outflow shadow part of it, causing the nebula to appear to have two offset lobes, as observed.

scattering models, while multiple scatterings may increase at shorter wavelengths. However, Yusef-Zadeh, Morris & White (1984) showed quite clearly that the effect of changing from single scattering to multiple scattering is like placing a diffusing screen in front of the nebula. The structure is simply blurred by the increased scattering, but the structure does not change. In summary, while individual images can be modelled moderately well with these scattering models, the detailed morphologies and the wavelength dependence are not matched in the case of AFGL2688.

Sixth, the standard model assumes that the bipolar outflow from AFGL2688 lies along an axis delineated by the N and S reflection lobes, at PA 15°. However, close examination of the images reveal that not only does the PA of the N and S lobes change with wavelength, but also the N and S lobes do not even lie on the same axis. We can determine the PA of the lobes from our IR images, either from the position of peak brightness or by determining the flux averaged center of brightness of the nebula along the RA direction defined as

$$\int_{-10.0}^{X} (X - x)^3 F(x) dx = \int_{X}^{+10.0} (x - X)^3 F(x) dx. \quad (1)$$

Here x is the R.A. position in arcseconds, X is the center of brightness position in arcseconds, and $F(x)$ the surface brightness at x. This function weights the center of brightness towards the region(s) of brightest emission. The RA center of brightness, plotted as a function of declination (DEC), then traces the axes of the lobes. In Fig. 7a–d for the J, 2.122μm (0.31″pixel scale), nbL and 10.0μm images, we plot the RA center of brightness position against DEC (solid line), and the R.A. position of the brightest point against DEC (dashed line). At each wavelength the results from the two methods are very similar. At J and 2.122μm both the N and S lobes apparently lie on an axis at PA≈5°, but there is a significant E-W offset between the symmetry axes of the N and S lobes – 2″at J dropping to about 1″at nbL. At nbL the axis of the S lobe is tilted about 7° with respect to the N lobe. In all the mid-IR images the N lobe is oriented at PA≈0°, and the S lobe at PA≈210°, but the axes of the two lobes join at the centre of the nebula. In the scattered near-IR continuum the two lobes are oriented more or less identically, but are offset tangentially from one another, whilst in the mid-IR thermal emission the two lobes point from a common origin but in entirely different directions.

4. A new model for the AFGL2688 nebula

We present in Fig. 8 a schematic view of our model for the AFGL2688 nebula, which is consistent with all the observations published to date. We interpret the set of knots and filaments which comprise the N and E blobs in Fig. 5 as a roughly circular loop of shock-excited emission. The bright knots at the N and E ends of the loop then probably represent limb brightening. The S and W blobs represent the limb brightened edges of another roughly circular loop. The loops represent the location at which the fast bipolar outflow is punching through one of the dense AGB mass loss shells seen in the I-band image of Latter et al. (1993). The loops are not complete, because of the highly clumped nature of the circumstellar environment which is seen very clearly in the E limb of the NE H_2 loop. The spacing of the concentric AGB shells in the Latter et al. I-band image is sufficiently close (∼3″) that within the radius of the outer, most prominent loop of H_2 emission we might expect to see another loop. There is indeed some evidence for this, since the complicated structure of the H_2 nebula is most easily explained if each cone in the biconical outflow contains two loops of shock excited H_2, spaced by ∼3″, as depicted in Fig. 8.

We interpret the H_2 ansae as shock-excited knots of emission arising where the fast bipolar outflow collides with the surrounding AGB wind, perhaps analogous to the FLIERs seen in some PN. The ansae then indicate the distance to which the

fast outflow has thus far penetrated. They are approximately 11″from the center of the nebula, in agreement with the result of Smith et al. (1990) who find that the high velocity component of the CO J=3-2 line extends to about 10″from the IR source. The spacing of the rings seen in the I-band image of Latter et al. (1993) is about 3″. Since the H_2 ansae appear at about 11″from the center of the nebula, we might expect to see three loops of shock-excited H_2 emission, where the fast wind punches through each of the three innermost rings (which we take to delineate dense, spherical, AGB mass-loss shells). While we do see two loops in H_2 (Fig. 8), a third loop is evidently not yet seen in H_2, which could indicate that the density of the AGB shell at this distance from the central star is too low to form a shock at the interface of the two winds. However, some compression is bound to occur at the interface, so that this may form a good scattering medium. The two offset axes of the optical nebula probably result from the overlap of two or three loops of compressed material, which forms a bright lobe of scattered continuum radiation.

If we assume that the two loops are approximately circular, then we can determine the geometry of the nebula from their projected dimensions and positions. The bipolar axis of the nebula in this model lies at a PA $\phi \approx 60°$ connecting the two H_2 ansae, and is inclined to the plane of the sky at an angle $\theta \approx 30°$.

The asymmetry in PA of the nebula observed in the continuum, and the horns so prominent at I and J, are also explained by this model. In Fig. 8, the bipolar axis of the nebula has a 30° inclination to the plane of the sky which causes the two H_2 loops to overlap from the observer's point of view. The N and S overlap regions delineate two axes, which run along the loops of H_2, at PA≈5°, with an E-W offset between them of ∼2″explaining the PA asymmetry and E-W offset between the symmetry axes of the N-S lobes. The models of Yusef-Zadeh, Morris & White (1984) and Latter et al. (1993) predict a pair of horns which, qualitatively, match those observed. In our model, a beam of radiation escapes from the star through the biconical regions carved out by the high velocity flow. These regions are filled with a low density, dusty medium. Limb brightening of the beam of radiation, scattered off the dust in the cavities, will generate horns, without the need for biconical cavities extending to large distances from the central star, which are needed by the "standard model", and which do not appear to be consistent with mm-wave CO maps.

One further important observation that must be explained is the apparent absence of any sign of scattered radiation from the E and W of the nebula, where we claim there are large openings into the bipolar cavities. One possibility is that, given that we have stated that the circumstellar environment is highly inhomogeneous, there is simply an absence of scattering material in these directions. A second, more likely, possibility is that the nebula is being asymmetrically illuminated. We have shown, by taking deeper images than have been published before, at a variety of wavelengths, that there is at least some scattered radiation from these directions. There is some faint extension at J along the entire western edge of the prominent N-S lobes. At K, even using a narrowband filter, this extension becomes more discernible (Fig. 4b), and there appears extension to the eastern edge as well as the western edge of the lobes. At nbL, at which wavelength some thermal emission from the nebula becomes important, a box-like structure of the shape required to fit our model is evident. In the mid-IR, where there is only thermal emission from dust, and no scattered continuum, the whole nebula is rectangular. As we progress to longer wavelengths, and we pass from the regime of scattered stellar continuum to thermal nebular dust emission, the nebula appears to rotate E of N. This spatial distribution of the thermal IR emission suggests that in fact there is material all around the large bipolar flow cavities, but it is not isotropically illuminated. This suggestion is further strengthened by the large scale of the shock-excited H_2 emission loops, which reveal the presence of material all around the flow cavities, albeit with some gaps due to the inhomogeneity of the circumstellar medium. The nebula could be asymmetrically illuminated if dense dusty blobs located close to the openings of the inner, dense torus, partially occlude the openings, shadowing the outer E-W parts of the nebula (Fig. 9). The concept embodied in Fig. 9 implies a significant degree of nebular asymmetry in the inner part of the nebula, which is indeed seen, both in scattered radiation at I and J, and in thermal emission in the mid-IR. In order to explain the observations exactly, the shadowing material would have to be to the NW of the opening on the SW side of the torus, and to the SE of the opening on the NE side, which implies a troublesome symmetry that we regard as a weakness in this model. This shadowing aspect of the model will be further discussed in Sect. 6. The dust temperature map (Fig. 6), as we mentioned earlier, can be interpreted as consistent with our new conceptual model.

5. Quantitative models for AFGL2688

In order to model the IR continuum emission we observe in AFGL2688, we have used a code which solves the radiative transfer problem for circumstellar dust shells in axial symmetry, and which was first described by Collison & Fix (1991; hereafter CF). The code treats absorption, reemission and scattering of radiation by grains in a torus of arbitrary optical depth. Scattering is presently assumed to be isotropic in the model, which is probably not as realistic as forward peaked scattering. Only a single grain size is used presently: multiple grain size models will be constructed in the future. We do not propose to generate models which explain every aspect of AFGL2688's spectral energy distribution (SED) and morphology. Instead, we present two models that demonstrate the gross morphological and SED differences between a model that is optically thin ($\tau_{10\mu m} \sim 0.4$) in the mid-IR and a model that is optically thick in the mid–IR ($\tau_{10\mu m} \sim 2.4$).

5.1. Description of model

The code is implemented as described by CF, with a few modifications. We have employed the slightly improved iteration scheme as described by Granato & Danese (1994). The density distribution in the envelope has been modified, and is now

described as

$$\begin{aligned}\rho(r,\theta) &= \rho_{\rm min} r^{-\rm B}(1+Ee^{[-(\frac{r}{r_{\rm sw}})^{\rm C}]})\times \\ &\quad (1+{\rm A}e^{[-(\frac{r}{r_{\rm sw}})^{\rm C}]}sin\theta) \qquad \text{for } \theta > \theta_\circ \\ &= D\rho_{\rm min} r^{-\rm B} \qquad \text{for } \theta < \theta_\circ \end{aligned} \tag{2}$$

where $\rho(r,\theta)$ is the dust grain number density at radius r and latitude θ, $\rho_{\rm min}$ the dust grain number density on the polar axis at the inner edge of the envelope, and A, B, C, D and E are user supplied constants. The wind of the AGB progenitor is assumed to have abruptly increased in strength by a factor 1+E at the termination of its AGB phase, as indicated in various other post-AGB stars (e.g. Skinner et al. 1994; Meixner et al. 1993, 1995). Prior to this stage the wind is spherically symmetric. As the star enters the 'superwind' phase, the wind becomes toroidal, and the resulting toroidal 'supershell' has a radius $r_{\rm sw}$ defined by Eq. (2). The equator to pole density contrast for the torus is a factor 1+A. The post-AGB fast wind has punched its way through the supershell, generating a low density bicone, and $\theta_\circ$ is the opening half-angle of the bicone. The dust grain number density at the inner edge of the envelope inside the bicone is actually $\rho_{\rm min}$D. The factor C determines how abruptly the mass-loss changed from an isotropic outflow at a modest rate to a toroidal superwind. The factor B is the usual geometrical dilution factor, equal to two for a constant mass-loss rate.

In addition to specifying the structure of the dustshell with the A,B,C,D and E parameters, we need to set the density of the dustshell by specifying an equatorial optical depth τ at a wavelength λ. For the density distribution given by Eq. 2, the value of $\rho_{\rm min}$ is now given by

$$\begin{aligned}\rho_{\rm min} &= \frac{\tau(1-B)}{\kappa}[r_{\rm min}(f_2{}^{1-B}-1)+ \\ &\quad r_{\rm min}{}^{B}E\{r_{\rm max}{}^{1-B}e^{-(\frac{r_{\rm max}}{r_{\rm sw}})^C}r_{\rm min}{}^{1-B}e^{-(\frac{r_{\rm min}}{r_{\rm sw}})^C} \\ &\quad +r_s{}^{1-B}(\gamma(\frac{1-B+C}{C},(\frac{r_{\rm max}}{r_{\rm sw}})^C) \\ &\quad -\gamma(\frac{1-B+C}{C},(\frac{r_{\rm min}}{r_{\rm sw}})^C))\}]^{-1}\end{aligned} \tag{3}$$

where $r_{\rm min}$ and $r_{\rm max}$ are the inner and outer radii of the envelope, f_2 is the ratio $\frac{r_{\rm max}}{r_{\rm min}}$, and κ is the mass absorption coefficient of the dust at wavelength λ. The function $\gamma(\nu,\mu)$ is the incomplete gamma function, for which accurate numerical solutions are straightforwardly obtained. The full radiative transfer equation is solved following the formalism of CF. As pointed out by Granato & Danese, when a density discontinuity is used, such as that at the boundary of the bicone cavities in our model of AFGL2688, it is important to set the boundary conditions on the points of the latitude grid on both sides of the discontinuity. For the current density distribution, the total mass of the envelope is given by

$$\begin{aligned}M &= \frac{2\pi\rho_{\rm min}r_{\rm min}{}^{B}}{3-B}(1-cos\theta_\circ)(r_{\rm max}{}^{3-B}-r_{\rm min}{}^{3-B}) \\ &\quad +2\pi\rho_{\rm min}r_{\rm min}{}^{B}\{\frac{2cos\theta_\circ}{3-B}(r_{\rm max}{}^{3-B}-r_{\rm min}{}^{3-B})\end{aligned}$$

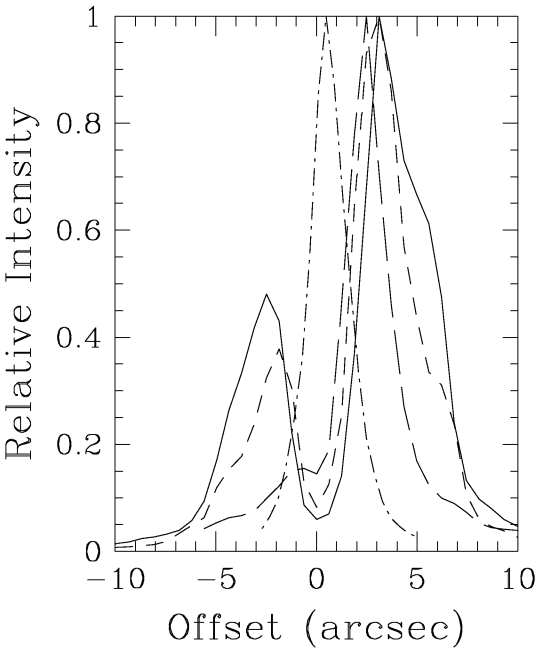

Fig. 10. Observed surface brightness of the nebula as a function of the offset from the star on the optical bipolar axis at 1.2μm (solid line), 2.104μm (short-dashed line), 3.4μm (long-dashed line) and 11.5μm (dot-dashed line).

$$\begin{aligned}&+\frac{A}{C}(\frac{\pi}{2}-\theta_\circ+sin\theta_\circ cos\theta_\circ)r_{\rm sw}{}^{3-B}[\gamma(\frac{3-B}{C},(\frac{r_{\rm max}}{r_{\rm sw}})^C) \\ &\qquad -\gamma(\frac{3-B}{C},(\frac{r_{\rm min}}{r_{\rm sw}})^C)] \\ &+\frac{2E}{C}cos\theta_\circ r_{\rm sw}{}^{3-B}[\gamma(\frac{3-B}{C},(\frac{r_{\rm max}}{r_{\rm sw}})^C) \\ &\qquad -\gamma(\frac{3-B}{C},(\frac{r_{\rm min}}{r_{\rm sw}})^C)] \\ &+\frac{AE}{C}(\frac{\pi}{2}-\theta_\circ+sin\theta_\circ cos\theta_\circ)r_{\rm sw}{}^{3-B}2^{(\frac{B-3}{C})}[\gamma(\frac{3-B}{C}, \\ &\qquad 2(\frac{r_{\rm max}}{r_{\rm sw}})^C)-\gamma(\frac{3-B}{C},2(\frac{r_{\rm min}}{r_{\rm sw}})^C)]\}\end{aligned} \tag{4}$$

which can be solved straightforwardly to a high degree of accuracy (better than 1 part in 10^6). (Note that there are no solutions to Eqs. 3 or 4 for B=1.00, nor to Eq. 4 for B=3.00: however, alternative equations can be derived if necessary to allow for a solution for these cases.)

We initially assumed a total luminosity for AFGL2688 of $1.4\times10^4{\rm L}_\odot$, and a stellar effective temperature of 6500K, consistent with Cohen & Kuhi (1977). We then varied the luminosity until a satisfactory fit to the observations could be obtained. The star is assumed here to emit like a blackbody. The dust is assumed to be entirely amorphous carbon, because the mid-IR spectrum of AFGL2688 is almost featureless (Justtanont et al. 1996). Optical constants for amorphous carbon have been taken from Hoare (1990). A single grain size is used in this model, and we have tried a variety of values.

We have three criteria we can use to judge the success of our AFGL2688 models. Firstly, we can compare the shape of the model nebula with the observations presented in Figs. 1 through 4 (Figs. 11 and 12). Secondly, we can compare radial profiles from the model with observations (Figs. 10, 11 and 12). Thirdly, we can compare the model SED with the observed photometry from the optical to the IR, where all the fluxes are integrated over the entire nebula. In Fig. 13, we plot observations from Ney et al. (1975), Latter et al. (1993), Justtanont et al. (1996) and Kleinmann et al. (1978). It should be noted in passing that AFGL2688 is known to have a strong feature in its spectrum, peaking close to 38μm, which may be attributable to a carbon based dust grain or MgS (Cox 1993), and the emission from this feature strongly affects the SED between about 20 and 60μm. We will not attempt to fit this feature in our models.

We use the same geometric parameters for both the optically thin and optically thick models. The value of 1+A (the equator-to-pole density contrast) is 4, the value of D (the inner bicone density factor) is 0.025 and the value of 1+E (the superwind mass-loss rate increase) is 20. The value of B (the geometric dilution factor) is 2. The value of C (sharpness of the superwind turn on) is 3. The grain size used for this model was 0.1μm. The opening angle of the biconical outflow is arbitrarily set to be 9° in this model, following the results of Latter et al. (1993).

5.2. Optically thin model

We present in Fig. 11 a model for AFGL2688 which is optically thin in the mid-IR. Specifically, at a wavelength of 10.0μm the optical depth is 0.4 in the equatorial plane. The inner radius of the torus was found to be 5000 stellar radii (3.3×10^{16}cm), which at a distance of 1.2kpc corresponds to 1.8″. We discuss the model's sensitvity to these parameters at the end of this subsection. This model predicts that at a wavelength of 3.4μm the nebula should be teardrop shaped, with FWHM roughly 4.5″, and with constant surface brightness over the central 3″or so. In the mid-IR the model predicts that we should see a slightly limb-brightened disk with radius roughly 3.6″. Both the model's 3.4μm and 9.8μm predictions are in clear contradiction to the observations. The core of the IR nebula is considerably more compact than this model would suggest, which confirms that indeed the optical depth of the nebula must be very large. Further confirmation comes from Fig. 13, where we plot the SED of the model. The model flux is reasonably close to the observations at most wavelengths. However, the hump in the model SED around 1–3μm is the reddened stellar photosphere: direct stellar radiation has not been shown in the maps in Fig. 11, because it greatly outshines the reflection nebulosity in the near-IR and optical. In a source with this low an optical depth, in the near-IR we would see a bright star, with a much fainter halo of nebulosity around it. To remedy the various deficiencies in this model, we must increase the optical depth at 10μm significantly. This result stands irrespective of the angle from which the torus is viewed. As the system is viewed from progressively closer to the polar axis, the central star becomes brighter relative to the nebula, and the nebula becomes more annular. Thus a low optical depth in the mid-IR is entirely ruled out.

5.3. Optically thick model

In Fig. 12 we present an optically thick model. In this model we find the inner radius of the torus to be only 1600 stellar radii (1.4×10^{16}cm), which is 0.76″at 1.2kpc). The optical depth at 10.0μm is now 2.4, and we see that the resulting morphologies are much closer to what is observed. The torus is no longer seen at any wavelength for which we have an image. Instead, the model nebula is elongated in the direction of the polar axes both in the mid- and near-IR. Comparison of the observed cross-cuts (Fig. 10b) and images (Fig. 1, 2, 3 and 4) with model predictions for the cross-cuts and images (both in Figs. 11 and 12) show fairly good agreement: the lobes steadily grow closer together, and the length of the nebula decreases, with increasing wavelength. The ratios of the brightnesses of the two lobes in the model are slightly larger than observed, but similar. All these details agree reasonably with the observations, although we should be wary of overinterpreting such details as these because, as we mentioned earlier, our model is assuming isotropic scattering and a single grain size, neither of which is likely to be realistic. Similarly, the appearance of horns in these model images should not be taken to be very significant – horns are produced relatively easily, and we do not regard the morphology we have used in our models as definitive. The SED produced by this model is shown in Fig. 14, and provides a fair fit to the observations. The scattering in the optical is somewhat excessive, and in the near-IR somewhat deficient due to our single grain size assumption. The model's central star is no longer directly seen in the SED, nor in the model images in agreement with observations. The length of the nebula at R is somewhat excessive (about 90″from end to end; Fig. 12), while at K it is somewhat too small (11″at the 1% level, compared with 16″in our observations). The dramatic reduction in size as we progress towards longer wavelengths would not occur if we adopted a distribution of grain sizes instead of a single grain size. The shape of the nebula at 3.4μm is again similar to what we observe, but the size is much smaller. At 9.8μm we generate a model with a length of about 4″, a little smaller than observed. Note that many of the sharp gradients in our model images would be smoothed out if we were to convolve with a circular PSF of FWHM 1.2″(nearly $2r_\circ$), as appropriate to our observations.

The only significant difference between the optically thick model and observations is at very long wavelengths (2600μm), where we predict a very small source, slightly elliptical and of order 3″in size. In contrast, the continuum regions detected by Yamamura et al. (1995) at 2.6mm and by Knapp et al. (1994) at 3.6cm are much larger with radii greater than 15″for the emission regions. We also underestimate the flux at these long wavelengths, detecting only about 50% of the flux seen by Yamamura et al., and a similar fraction of that seen by Knapp et al. One possible explanation for the model's underestimate is that our pre-superwind mass loss rate is too low or varies in intensity. It is also possible that some fraction of the extended emission

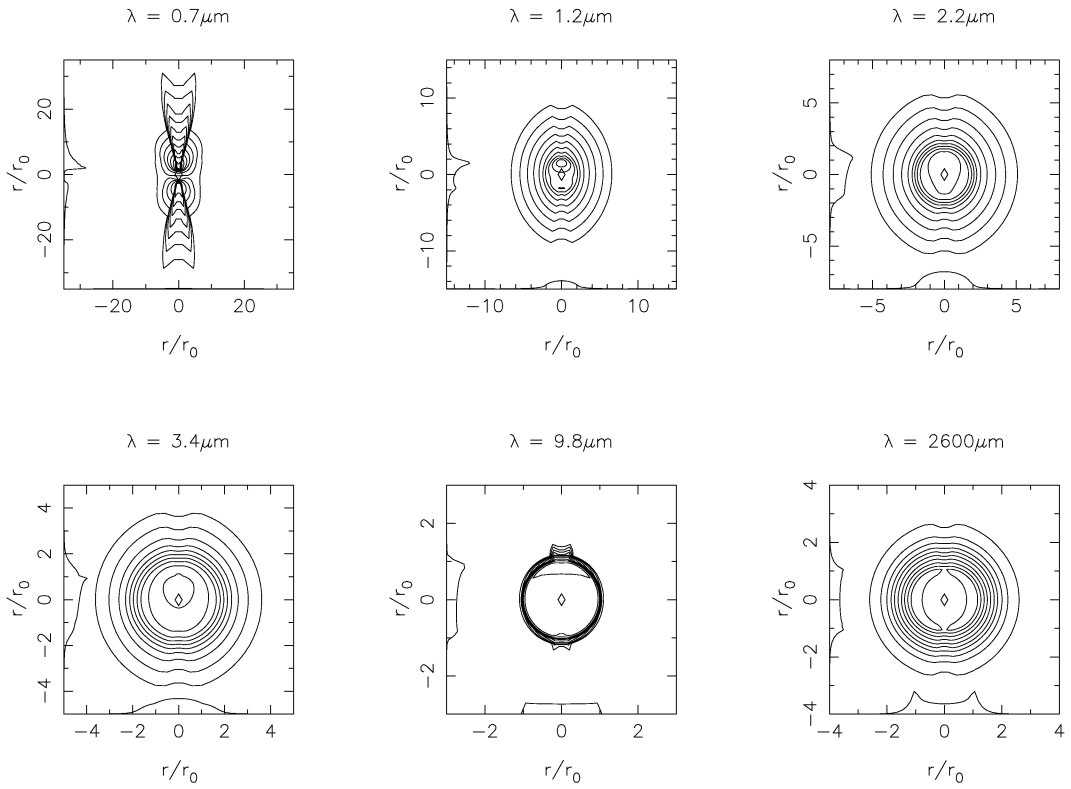

Fig. 11a. Model surface brightness maps at a variety of wavelengths. In each panel the contour maps have logarithmically spaced levels from 1% to 100% of the peak surface brightness. Note that direct stellar radiation is *not* shown in these figures, and this contribution would grossly outshine the nebula in the near-IR. On the right hand side of the panel is a surface brightness cross-cut through the nebula along the bipolar axis, while at the bottom is shown a cross-cut through the nebula in the equatorial plane; the crosscuts are linear in flux. These cross-cuts can be compared to those through the observed images which are presented in Fig. 10. The axes for the plots are scaled in units of $r_\circ$, the inner radius of the superwind (see text for values for $r_\circ$). A diamond indicates the position of the central star, and the wavelength for each model image is shown above the panel. The model shown here, as discussed in the text, has an equatorial optical depth at 10μm of 0.4, and $r_\circ$ corresponds to 1.85″.

seen at 3.6cm is due to molecular line emission included within the spectral bandpass, although there are no obvious candidates for a molecule heavy enough and abundant enough to generate the required emission at these wavelengths. Nevertheless, our purpose here in presenting our current modelling efforts is to demonstrate that the AFGL2688 torus *must* be optically thick at 10μm, and that a superwind plus spherical AGB wind model can plausibly reproduce the observed general characteristics of the nebula. We will further investigate the physical structure of the AFGL2688 nebula in much more detail in a forthcoming paper.

5.4. Constraints on models

Our model contains many parameters, some of which are well constrained, and others less so. Here we describe our model's sensitivity to some of the important parameters. The lower density biconical sections described by $\theta_\circ$ and D are important. Our observations of H_2 imply that a fast wind has indeed carved out cavities in the nebula. The 'waist' seen in the optical and near-IR images demands an extremely large equatorial optical depth for this system, yet the very large reflection nebula requires a rather low optical depth in the direction of the lobes. The amount of scattered radiation, which fully determines the SED in the optical and near-IR, is very sensitive to the value of the parameters D (the inner bicone density factor) and $\theta_\circ$ (the bicone opening half-angle). The value of B (the density geometric dilution factor) we have left at 2, consistent with a constant mass loss rate. Any other value would imply a slowly time-varying mass loss rate. The value of r_{min} (the supershell inner radius) has a strong effect on the colour of the dust emission spectrum, and r_{sw} (the toroidal supershell outer radius) significantly affects the separation of the reflection lobes, and both are well constrained by our data. The value of E (the superwind mass-loss rate increase) has a large effect on the size of the reflection nebula, and can be well constrained. Models without a large amplification in mass loss rate in the superwind tend to produce excessive flux in the far-IR, and require a larger total mass in the envelope to fit the SED. Such models also tend to produce a rather extended nebula in the 10 and 20μm regions, compared with the fairly compact source which we observe at wavelengths as long as 19.2μm. The value of A (1+A is the equator to pole density ratio) is not very well constrained. Varying A has some effect

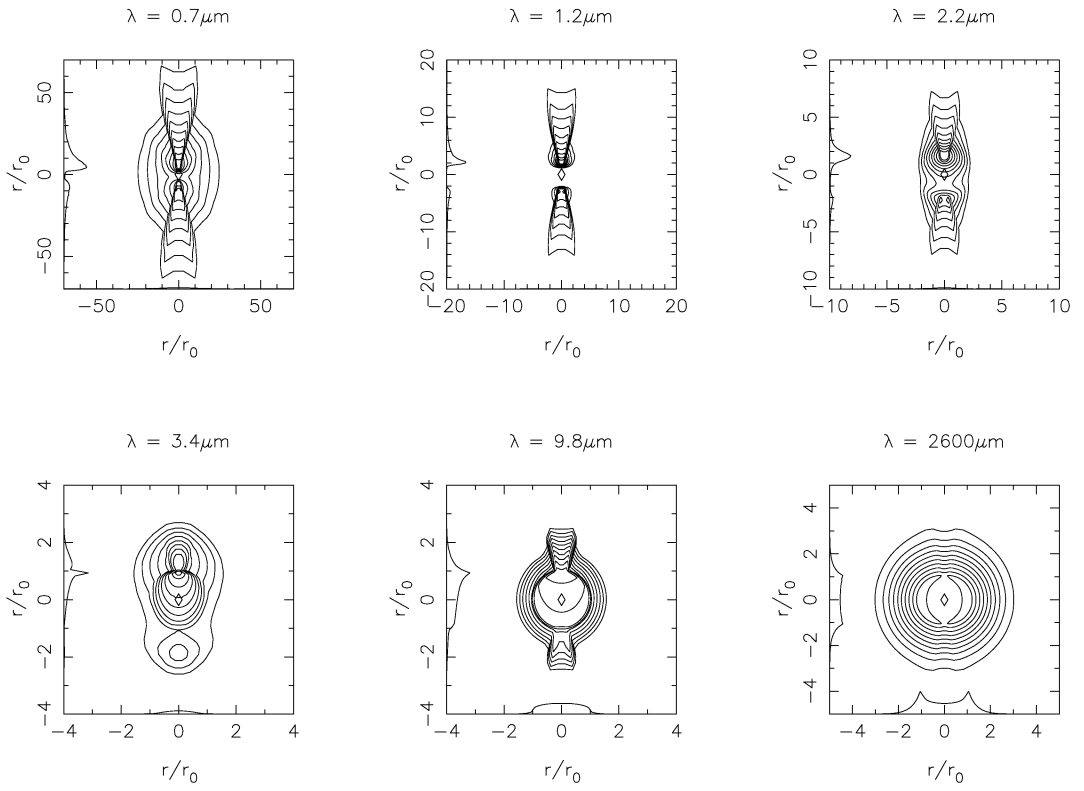

Fig. 11b. The same as Fig. 11, but this model has an equatorial optical depth at 10μm of 2.4, and $r_\circ$ corresponds to 0.77″.

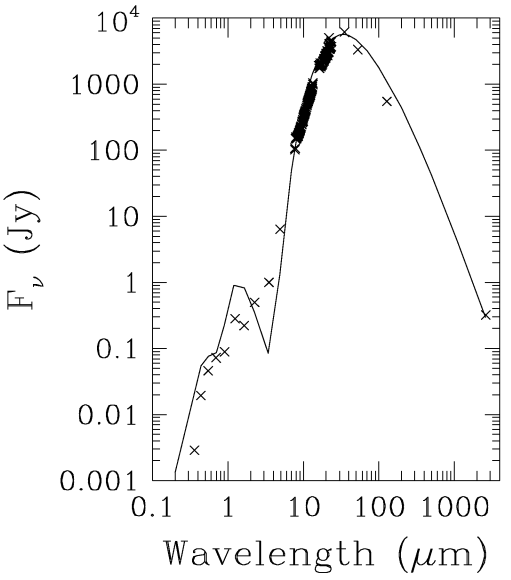

Fig. 12a. Model SED compared with observations (crosses). This is the model illustrated in Fig. 11, viewed from an inclination angle of 25° away from edge-on.

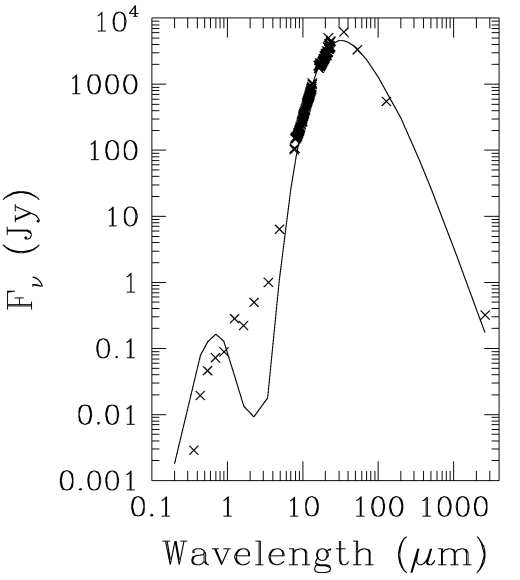

Fig. 12b. The same as for Fig. 13, but for the model illustrated in Fig. 12, viewed from 25° away from edge-on.

on the slope and width of the SED of the dust shell, but the effect is not particularly pronounced when the optical depth is so large. The values of A, D and $\theta_\circ$ are not independent, but the images and SED provide separate constraints on these three parameters. Finally, we note that the luminosity of our model is much larger than the $1.3\times10^4 L_\odot$ determined by Cohen & Kuhi (1977) (corrected for the different distance which they assumed), but they pointed out that their luminosity estimate (which was based on the SED, under the assumption that the

torus was optically thin in the mid-IR) was highly uncertain because of the unknown physical structure of the nebula. Because our model has a strong departure from spherical symmetry that allows radiation to escape easily in the polar directions, while in the equatorial direction we only see multiply reprocessed radiation emerging from the dust shell, the apparent luminosity of AFGL2688 is dependent on viewing angle.

5.5. Derived physical parameters

In Table 2, we list some physical parameters derived from our model. As stated before, we stress that these are not intended to be definitive, but to give a reasonable indication of the likely values, consistent with the model we have qualitatively sketched out in the previous section. All masses are derived assuming a gas-to-dust ratio of 200 by mass, and a constant outflow velocity of 22.4km/sec throughout the nebula. The inner radius in this model implies that large scale mass loss stopped about 190 years ago. The model contains a total mass of nearly $5M_{\odot}$ of material, but the mass distribution beyond the supershell has not yet been well constrained. The mass required in the supershell alone, however, suggests that the progenitor must have had a fairly high mass, toward the high end of the mass range for AGB stars.

6. Discussion

6.1. Morphology

The standard model for AFGL2688 does not explain the offset between the N and S reflection lobes, the kinematics of the H_2 emission, the ansae seen in H_2 or the morphology of the H_2 emission. Our alternative model is designed to explain all these results. Nor can the standard model account for the rectangular appearance of the nebula at low surface brightness levels in the near-IR and mid-IR. Such a morphology also arises quite naturally in our model.

The model presented here for AFGL2688 is certainly very different from the 'standard model', and initially some aspects, for example the inhomogeneity of the nebula and its asymmetry, may seem unattractive. Such clumpiness as we postulate here has in fact already been inferred from observations of AFGL2688 and its cousin AFGL618. Schmidt & Cohen (1981) discussed spectropolarimetry of the lobes of the bipolar nebula AFGL618. They observed both ionized and neutral species in the lobes, and concluded that the lobes must bear a fast, hot wind responsible for the ionic lines, but there must be embedded in it denser condensations inside which and in whose shadows various neutral and molecular species could exist. Cernicharo et al. (1989) observed a rich variety of molecules in the outflow of AFGL618, many of which were seen at very high velocity, suggesting that they were in the fast wind. The relatively hard radiation field from the central star of AFGL618 in the lobes should photodissociate molecules in the fast wind, and their reformation ought to be suppressed by the low density at points where the temperature in the wind could be low enough for molecule formation. The existence of dense clumps in the wind could allow the formation of molecules. Likewise, in the bipolar lobes of AFGL2688, spectropolarimetry by Cohen & Kuhi (1977) indicated the existence of C_2 in two different density regimes, once again indicating that there are probably dense clumps in the lobes. They speculated that the clumps may even allow the condensation of C-rich grains inside the bipolar lobes. The structure of the inner 'blob' of H_2 to the east of AFGL2688 strongly suggests a filament consisting of a series of large clumps. The mid-IR images of the young PN IRAS21282+5050 presented by Meixner et al. (1993), and the mm-wave interferometer images of the same source (Shibata et al., 1989) indicate that its envelope is extremely clumpy, and the inhomogeneity exists on rather large scales. Finally, the same conclusion is reached from the variety of images presented by Graham et al. (1993) of the prototypical young PN NGC7027. Thus a large degree of inhomogeneity is seen in a variety of well resolved post-AGB nebulae and young PN.

The asymmetry of the nebula, in particular the appearance of the optical lobes over towards one edge of each cone in the bipolar outflow, may seem worrisome. In fact, once again the young PN NGC7027, and the extensive observations of it by Graham et al. (1993), should be examined. Both the inner and outer loops of H_2 in NGC7027 are asymmetric. The inner loop is almost a complete ring. The outer loop exhibits a similar asymmetry to that seen in AFGL2688 – specifically, the H_2 appears concentrated in two opposing corners of a box structure, and offset from the apparent axis of a bipolar outflow. If we were to evolve this PN backwards in time as far as the point when it had just recently left the AGB, we could well see a structure very much like that which we see in AFGL2688. In fact, if we examine any of the near-IR images of NGC7027 presented by Graham et al. (1993), we see a remarkable similarity in shape to the box-like nebula we see around AFGL2688 in the mid-IR, or at low flux levels even in the near-IR in the L and K bands.

Remarkably, shortly before completing the manuscript of this paper, we received a preprint discussing new ^{13}CO images of AFGL2688 (Yamamura et al. 1995), which provides strong support for our model. Yamamura et al. find that the ^{13}CO emission, which is optically thin, consists of three components – a bright, circular core, a fainter more extended halo, and higher velocity components. The core is unresolved and so the toroidal structure which we expect to be present must be smaller than about 4″in size, which is consistent with our dust model. The higher velocity components (corresponding to the 'medium velocity wind' discussed by Young et al. 1992) consist of two red- and blue-shifted lobes separated by about 3″on an axis at PA $\sim 60^{\circ}$ – exactly the PA we claim for the bipolar flow. The shapes and sizes of the ^{13}CO high velocity lobes are such that they fit nicely inside the biconical structures which we have proposed are delineated by the H_2 emission, beautifully confirming the presence of gas streaming at high velocity in the large bipolar flows as we predict. The ^{13}CO emission is shown overlaid on our H_2 image in Fig. 15. The high velocity lobes appear to be resolved, and so seem to confirm our suggestion that the opening angle of the bipolar flow is very large. The considerable overlap

Table 2. Physical parameters and results for models

Parameter	Thick Model	Thin Model
T_{eff}	6500K	6500K
Stellar radius	8.5×10^{12}cm	6.5×10^{12}cm
Luminosity	$2.7\times10^{4}L_{\odot}$	$1.6\times10^{4}L_{\odot}$
Distance	1.2kpc	1.2kpc
Mass-loss rate in superwind	$3.9\times10^{-3}M_{\odot}$/yr	$1.9\times10^{-3}M_{\odot}$/yr
Superwind duration	190 yrs	230 yrs
Total mass in supershell	$0.76M_{\odot}$	$0.43M_{\odot}$
Mass-loss rate on AGB	$1.1\times10^{-4}M_{\odot}$/yr	$7.1\times10^{-5}M_{\odot}$/yr
Total mass in AGB wind	$2.2M_{\odot}$	$3.2M_{\odot}$
Assumed gas-to-dust ratio by mass	200	200
Outflow velocity	22.4km/sec	22.4km/sec
Time since major mass loss terminated	190 years	230 years
Inclination of bipolar flow axis to sky	25°	25°
Equatorial $\tau(10.0\mu m)$	2.4	0.4
A	3	3
B	2	2
C	3	3
D	0.025	0.025
E	19	19
$\theta_{\circ}$	9°	9°

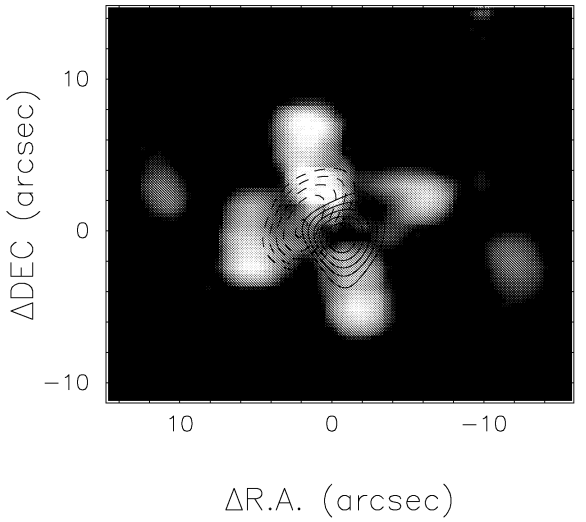

Fig. 13. Pure molecular hydrogen emission taken from Fig. 5, with overlaid on it the red-shifted (solid contours) and blue-shifted (dashed contours) high velocity ^{13}CO emission observed with the Nobeyama Millimetre Interferometer by Yamamura et al. (1995). The ^{13}CO and H_2 emission both appear to delineate a bipolar flow at a position angle of about 60°.

of the two lobes also implies a significant angle between the axis of the flow and the plane of the sky, as we have suggested.

6.2. CO emission

The observations by Yamamura et al. (1995) described above strongly suggest that the interpretation of CO line profiles of the type displayed by AFGL2688 should be thought about very carefully. First of all, we note in passing that the bipolar flow speed appears to have previously been calculated incorrectly for AFGL2688 (Young et al. 1992) and for AFGL618 (Cernicharo et al. 1989). These authors have assumed that the maximum velocity observed in faint wings in the CO line profiles of these objects represents the projected bipolar flow speed. They have then divided the maximum observed velocity by the sine of the angle of inclination of the bipolar flow axis to the plane of the sky. However, the geometric term which should have been employed is not just the angle of inclination of the bipolar axis to the plane of the sky, but this angle summed with the half angle of the bicone, in order to allow for the projection effects of the finite opening angle of the bicones. (See Fig. 16 for an explanation.) Using this procedure, the inclination angle of the bipolar axis in our model (25°) should be added to the large cone opening half-angle (∼50°) in order to determine the maximum velocity which will be seen in the bipolar flow region, which is then $v_{bip}/sin75°$. Given the maximum velocity of 100km/sec determined by Young et al. (1992), the bipolar flow speed v_{bip} is then ∼100km/sec. This is not much different from the bipolar flow speed seen in the binary system OH231.8+4.2 (Morris et al. 1987), depending on the uncertain inclination angle in that system, and is an altogether much more reasonable result than those quoted earlier for AFGL2688. In AFGL618, if we adopt the half angle of 10° determined by Latter et al. (1992), the overall angle is then 55° rather than 45°, reducing the bipolar flow speed from 270km/sec to 190km/sec. However, the single scattering models used by Latter et al. (1993) appear to underestimate the inclination and opening angles compared to the multiple scattering models of Yusef-Zadeh, Morris & White (1984) and, thus, the bipolar flow speed in AFGL618 could be lower yet than 190km/sec.

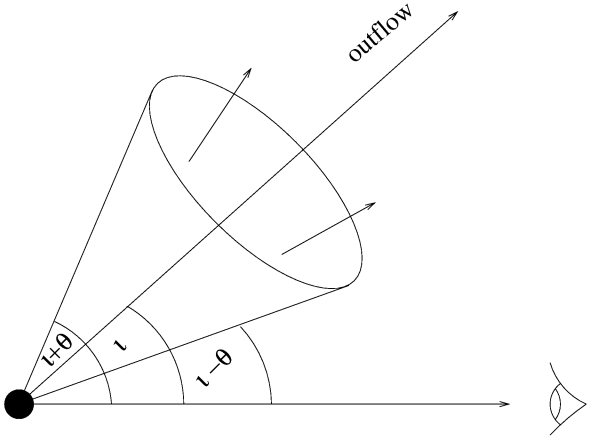

Fig. 14. Schematic view of a conical outflow, viewed at an inclination angle ι. A wind is assumed to flow radially outward through the cone, from a star which is indicated by the black circle, at a velocity v. The opening half-angle of the cone is θ, and the direction of the conical outflow is indicated, as well as the line of sight. It is easily seen that the projected velocity of material in the outflow observed spectroscopically will vary between a minimum value of $v\cos(\iota+\theta)$ and a maximum value of $v\cos(\iota-\theta)$.

More importantly though, we wish to point out that the rather faint and very broad wings seen in the CO lines of a number of post-AGB stars do not in any case appear consistent with an interpretation in terms of bipolar flows (even if the velocity calculations are done correctly). We illustrate the problem in Fig. 17. A uniformly expanding, optically thick, spherical outflow, with velocity V_s, as pertains to the typical AGB star, generates a roughly parabolic CO line with full width at zero intensity of $2v_s$ (Fig. 17a). In a simple kinematic model comprising such a slow, isotropic outflow, plus a well collimated, fast, bipolar flow, with tiny opening angle and flow speed v, on an axis inclined at angle ι to the line of sight, we see once again the standard parabolic profile, plus two narrow components at velocities of $\pm v\cos\iota$ (Fig. 17b; we assume the central star to have zero velocity in the local standard of rest). Finally, if we now allow the bipolar outflow to be biconical with reasonable cone opening angles, the two narrow features are broadened by projection, so that the composite line profile for such an object is as depicted in Fig. 17c, comprising *three* distinct features. In practise, no such line profile has been observed in any of the post-AGB sources. Instead, what are observed are standard AGB type line profiles plus very broad wings which appear to be more or less Gaussian, peaking close to the systemic velocity. It is easy to see in Fig. 17 that if the angle ι approaches 90°, so that the bipolar axis lies roughly in the plane of the sky, then the two peaks generated by the bipolar flow in the CO line profiles will lie on top of one another, and the result will indeed be simply broad wings either side of the AGB wind profile, as observed in the case of AFGL2688. As mentioned earlier, the near-IR images do not appear consistent with an axially symmetric structure with an axis in the plane of the sky, but instead imply an inclination angle of more like 25°. At such an inclination angle, and with a bipolar flow speed of 100km/sec, the two bipolar flow spectral features would peak around 45km/sec to each side of the center of the AGB wind profile. This is not entirely ruled out by the observations, but does appear unlikely. However, in the case of AFGL618 the much larger inclination angle (45°) and bipolar flow speed (190km/sec) mean that the two bipolar flow peaks should be clearly seen in CO line profiles, and so in this case the spectra are quite inconsistent with a bipolar flow model. The same applies to OH231.8+4.2. The fact that no such features are seen in any of these sources would imply that the bipolar flow axis lies very close to the plane of the sky in every case, which statistically is of course highly unlikely. In the observations of Yamamura et al. (1995) we clearly see the bipolar flow from AFGL2688 (Fig. 15). The bipolar flow is seen at velocities consistent with the 'medium velocity wind' component described by Young et al. (1992). Given that this 'medium volcity' component is actually the bipolar flow, and given our inclination and opening angles, the two bipolar flow peaks in the CO line profiles should be so close together that they will lie on the AGB wind part of the profile, and thus be very difficult to identify. Neri et al. (1993) suggested that the very broad wings in the molecular line profiles of AFGL618 were basically generated thermally by hot, post-shock gas, rather than kinematically in a wind, and we suggest that this proposal by Neri et al. very nicely explains the CO line profiles in AFGL2688 also. Thus in our model the 'low velocity wind' of Young et al. (1992) corresponds to the spherical AGB wind, the 'medium velocity wind' to the bipolar flow observed by Yamamura et al., and the 'high velocity wind' to hot, possibly post-shock gas. The latter component may be identified with the region of shocked molecular hydrogen emission (Fig. 5, 15), but there are other possibilities just as outlined by Neri et al. for the case of AFGL618. The fact that the 'high velocity' component appears to become steadily stronger, relative to the 'low velocity' component, with increasing rotational transition in the CO observations of AFGL2688 by Young et al. (1992), is consistent with our suggestion that the 'high velocity' component arises in hot gas. Furthermore, the high rotational lines observed in AFGL2688 by Justtanont et al. (1997) demand very warm and dense gas which can realistically only be provided by a Photo-Dissociation Region or a shock. Thus all the available CO data appear to be consistent with this model.

CO maps (Truong-Bach et al. 1990; Yamamura et al. 1995) of AFGL2688 show that the overall density distribution of the outer AGB wind is spherically symmetric, with which our model is entirely consistent. The scattering models of Yusef-Zadeh, Morris & White (1984) and Latter et al. (1993), on the contrary, take the density distribution of the entire envelope to be equatorially peaked, with evacuated biconical cavities extending throughout the envelope. This appears unrealistic since, as mentioned before, the available evidence suggests that AGB winds are more or less spherically symmetric, and that in this source the biconical flow regions only extend a small distance through the envelope. For realism these scattering models should take low density cones carved through a spherically symmetric envelope with the usual r^{-2} law of density. Bieging & Rieu (1988)

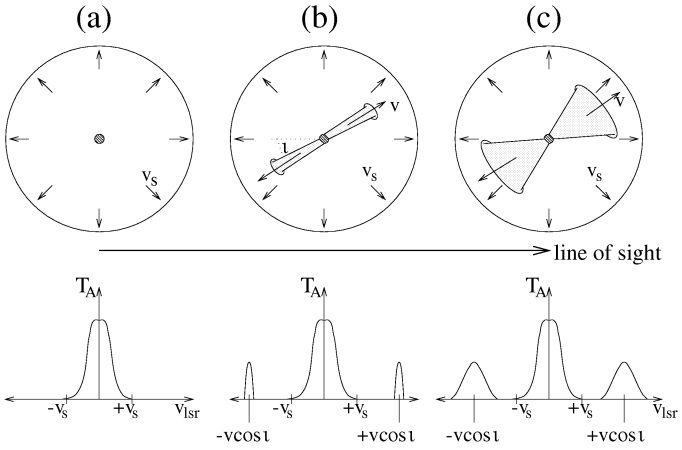

Fig. 15. Formation of CO line profiles in outflows. The upper diagrams illustrate three different outflow morphologies, and the diagram below each illustrates schematically the type of line profile to be expected. **a**: an optically thick spherical outflow, as generated by most AGB stars, gives rise to a parabolic line profile. **b**: morphology as **a**, with the addition of a bipolar flow with vanishingly small opening angle. This yields the standard AGB star parabolic line profile, with two very narrow features either side at the projected velocities of the bipolar flow. **c**: morphology as **b**, except now the bipolar flow is biconical with non-negligible opening angles. The two spectral features due to the bipolar flow are broadened by projection due to the cone opening angle.

claimed the existence of a rotating toroid from their HCN interferometer data. Their maps did not clearly resolve a toroid, indicating that it can only be at most a few arc seconds in diameter. An unambiguous determination of the geometry of the AFGL2688 nebula will have to await interferometers with high enough spatial resolution to fully resolve the central torus (whose presence is always assumed), for instance in HCN (a tracer of warm, high density gas), and/or through the use of high enough sensitivity to map the high velocity flow, which is very faint, in CO.

The spherically symmetric CO maps mentioned above are important. The low excitation CO rotational lines (e.g. J=1-0) imply a mass-loss rate of order 10^{-4}M$_\odot$/yr (Morris 1980; Knapp et al. 1982; Knapp & Morris 1985). This is in reasonable agreement with the value for the AGB wind which we have used in our radiative transfer model. For mass-loss rates in this range, the excitation of CO is entirely collisional (Justtanont, Skinner & Tielens 1994), and so the CO maps reflect the density structure of the AGB wind. Thus these maps strongly suggest that AFGL2688's envelope is mostly quite spherical, except for the superwind at its core. The dust on the other hand is entirely radiatively excited, and so the combination of dust and gas maps allows us to resolve the effects of temperature and density on the appearance of the nebula.

6.3. Thermal pulsing during the AGB phase

The possible connections between helium shell flashes (thermal pulses) in AGB stars and the ejection of planetary nebulae have been reviewed by Wood & Vassiliadis (1993). The duration of the energy generation peak that is associated with the helium shell flash is of the order of 100-200 years (see e.g. Fig. 5 of Iben 1983), while diffusion through the star can spread the associated surface luminosity spike out over a timescale of ∼500 years (Wood & Vassiliadis 1993). Wood & Faulkner (1986) noted that for sufficiently massive AGB stars the luminosity at a helium shell flash could exceed the Eddington luminosity L$_{ed}$ at the edge of the core, such that no hydrostatic solution for the envelope could exist, with the likely result of complete envelope ejection. They showed that L > L$_{ed}$ could occur at the peak of the luminosity spike in AGB stars having a degenerate core mass ≥0.9 M$_\odot$, provided the envelope mass was ≤1.5 M$_\odot$. Thus Wood & Vassiliadis (1993) noted that degenerate core masses ≥0.9 M$_\odot$ are only likely to develop in AGB stars with a total mass ≥5 M$_\odot$ (so that the initial envelope mass would have been ≥4 M$_\odot$), but that the radiation pressure mechanism could only act to remove ≤1.5M$_\odot$ of envelope material.

The above requirements are in excellent agreement with the masses and timescales that we have derived for AFGL2688. The current luminosity of 2.7×10^4 L$_\odot$ estimated for AFGL2688 (Table 2) implies a relatively high core mass for the central object – if it is currently hydrogen-shell burning, the core mass versus luminosity relation of Vassiliadis & Wood (1994) implies a core mass of 0.98 M$_\odot$, while the helium-shell burning tracks of Wood & Faulkner (1986) yield a similar mass. The derived supershell mass of 0.76 M$_\odot$ (Table 2) and its ejection timescale of ∼200 years are consistent with ejection by a super-Eddington luminosity spike following a helium shell-flash. Our estimate of 2.2 M$_\odot$ for the total mass ejected by the preceding AGB wind (Table 2), together with the supershell mass of 0.72 M$_\odot$ and the current degenerate core mass of 1 M$_\odot$ imply an initial AGB mass of >4 M$_\odot$ for the precursor (our model only includes mass lost from the star within the last 2×10^4yrs, and its AGB lifetime is likely to have been many times longer than this), consistent with the requirement above that the initial AGB mass should have exceeded 5 M$_\odot$.

Despite the good agreement between our derived mass-loss parameters for AFGL2688 and thermal pulse theory as outlined above, the theory currently cannot explain the toroidal geometry found in the supershells of AFGL2688 and other post-AGB objects.

6.4. Magnetic fields

One of the mechanisms which might possibly be invoked to explain the toroidal morphologies of post-AGB star supershells is focussing of an outflow by a magnetic field. Hu et al. (1993) have commented on the possible effects of magnetic fields on the evolution of post-AGB nebulae. They suggest that closed magnetic field lines around the stellar equatorial region could restrict the outflow of material in the equatorial region, leading to a build-up of dense material in the equatorial plane, which indeed is what is observed in many post-AGB nebulae. Nothing is known about the dynamo which generates stellar magnetic fields, so that any discussion of the likely behaviour of, and ef-

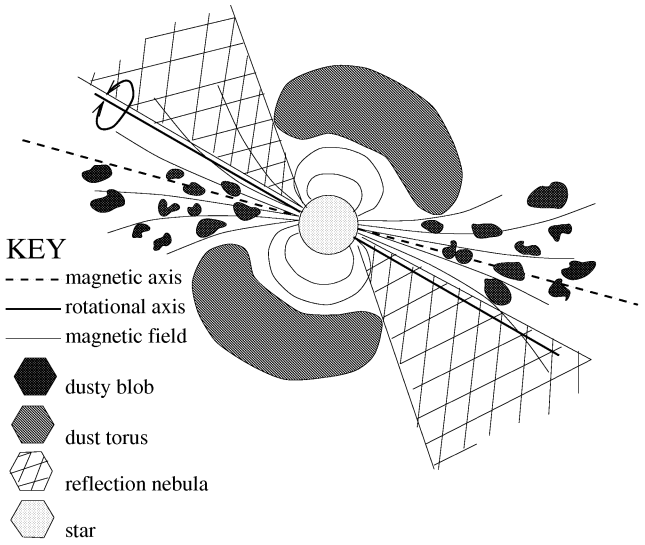

Fig. 16. Schematic view of the inner region of the AFGL2688 nebula showing a means by which the outflow could be magnetically directed leading to the observed brightness distribution.

fects of, magnetic fields during AGB and post-AGB evolution can only be treated as speculation at present. The simple calculations of kinetic and magnetic energy flux densities in the case of the PPN IRAS17150–3224 by Hu et al. (1993) may be extended to the case of AFGL2688 very straightforwardly. Bieging & Rieu (1988) suggest a magnetic field strength at the surface of the AFGL2688 central star of ∼3kG. If we assume that the magnetic dipole has remained functioning in the same manner and with the same efficiency throughout late AGB and post-AGB evolution of this star, assume that the magnetic field through the stellar envelope acts like a dipole, extrapolate back in time to the AGB, and assume a standard AGB luminosity of $\sim 6000 L_{\odot}$, the magnetic field strength at the surface of the AGB star would have been ∼100G, entirely consistent with magnetic field strengths measured in the winds of OH/IR stars by circular polarisation of OH and SiO maser lines (e.g. Cohen 1989; Barvainis, McIntosh & Predmore 1987). In the superwind phase, the stellar wind would have been so dense that the gas kinetic energy density was probably very much greater than the magnetic energy density, so that the magnetic field can have had little influence on the outflow. In the post-AGB phase, however, things may well have become very different. For the magnetic field to dominate the gas flow characteristics, it is a necessary condition that $\frac{1}{2} n_H m_H v_w^2 << B^2/8\pi$ for a system like AFGL2688 where the outflow is presumably mostly neutral. At the stellar surface, if we take B=3kG, v_w=40km/sec (similar to the medium velocity outflow component of Young et al. 1992) and $\dot{M} \sim 10^{-6} M_{\odot}$/yr, this condition is certainly satisfied. In the equatorial region, continued outflow from the warm central star can then be impeded, whilst in the polar direction the magnetic field lines are more or less open and allow gas to flow away rapidly in a bipolar fashion. If the magnetic polar axis were offset from the star's rotational axis, then the axes along which ejected material preferentially flows would precess about the rotational axis. Clumps of dust forming in the bipolar flow would then arise preferentially in a direction offset from the rotational axis, and lead to opposing sides of the bipolar nebula being shadowed. Such a scenario would account for the geometry of the AFGL2688 nebula (see Fig. 18), but we stress that while there is observational justification for much of this idea, it must currently remain as conjecture. The spatial resolution of the Keck Telescope at 20μm may be sufficient to investigate this hypothesis observationally (a wavelength as long as 20μm is needed because at shorter wavelengths the nebula is optically thick). Intuitively an offset between the rotational and magnetic polar axes sounds unlikely. However, we repeat that the stellar magnetic dynamo is not understood yet, and there is some evidence in a number of pre-main sequence stars for precessing, magnetically confined, bipolar jets (e.g. Lightfoot & Glencross, 1986). In such systems the 'jet' follows a helical path away from the star because of the precession of the magnetic polar axis. However, very tight collimation is required to obtain a helical jet such as that in HH7–11 (Lightfoot & Glencross, 1986).

6.5. Relationship to other bipolar nebulae

AFGL2688 is not the first post-AGB nebula to show asymmetric structure. The young PN M1-16 has a strongly bipolar outflow, but the axis of the outflow as seen in H_2 is at a substantial angle to that suggested by optical images (Aspin et al 1993). This suggests that asymmetric outflows such as that in AFGL2688 might not be unusual. Moreover helical outflows in post-AGB stars may not be rare either: we point out that many of the bipolar PN studied by Corradi & Schwarz (1993) have position-velocity diagrams with sinusoidal patterns along the long slit of their spectrometer. The simplest explanation for such sinusoidal patterns is that the outflow structures are helical. Of course this would not necessarily imply that material flows along a helical path. If the outflow were to some extent magnetically confined close to the star, we need not expect it to remain such as it reaches larger distances from the star. The helical pattern then simply represents a record of the direction of the magnetic polar axis at the time the material was ejected from the star.

Spectacular bipolar post-AGB nebulae such as AFGL2688 are rare. There are four well known examples — AFGL2688, AFGL618, AFGL915 (the Red Rectangle) and Roberts 22. Another fainter member of this class, IRAS17150–3224, has only recently been discovered (Hu et al., 1993). There are many more post-AGB stars which optically appear point-like, although they may have extended thermally emitting nebulosity in the IR. One might suppose that the bipolar nebula is a phase which many stars pass through but only briefly. However, AFGL618 has evolved almost to the status of a young PN, and yet still retains its optical bipolar nebula. Next there is the possibility that the point-like and bipolar post-AGB nebulae are the same class of objects viewed from different angles. The relative numbers of objects then dictate that most post-AGB stars must have geometrically very thin, but dense, disks, so that the bipolar nebulae could only be tipped very slightly away from edge-on. The large inclination angle suggested for OH231.8+4.2 (47°),

AFGL618 (45°) and AFGL2688 (25°) rule out this possibility. Finally, we are left with the possibility that only a very few post-AGB stars generate spectacular bipolar nebulae. AFGL2688 and AFGL618 are both extraordinarily heavily obscured for such evolved stars, and whilst most post-AGB stars have observable CO lines in their mm-wave and sub-mm spectra, these two have remarkably strong lines, implying that they had very large AGB mass loss rates. All these facts point towards the bipolar post-AGB nebulae being descendants of the most massive AGB stars, as are the Type I PN (Peimbert 1978). NGC7027, whose similarities to AFGL2688 have been commented on earlier, has one of the hottest PN central stars and a very high excitation and very massive nebula. It is presumably likewise descended from a relatively massive AGB star, and we speculate that AFGL2688 and GL618 will both evolve into PN similar to NGC7027.

6.6. The case of the missing UIR bands

Among the currently known C-rich post-AGB stars, AFGL2688 is unusual in being almost the only one with very weak UIR band emission. The Red Rectangle, for example, has strong UIR band emission throughout its IR spectrum. The 21μm sources are a growing group of post-AGB stars discovered on the basis of their unusual mid-IR spectra (Kwok, Volk & Hrivnak 1989; Justtanont et al. 1996), which are dominated by very broad emission features attributed to hydrocarbon molecular groups. AFGL2688, in contrast, has an almost featureless mid-IR spectrum apart from a possible weak emission feature around 8μm (Fig. 14). Why should AFGL2688 be so different to its C-rich cousins in this respect?

Most of the sources so far shown to exhibit the UIR bands have warm or hot exciting stars. These sources include post-AGB stars, PN, HII regions and reflection nebulae associated with young stars. In almost all of these objects, the radiation field includes a substantial flux of UV photons. The UIR bands are usually attributed to hydrocarbon containing materials, either PAHs (Polycyclic Aromatic Hydrocarbons) or HAC (Hydrogenated Amorphous Carbon). In either case, the generation of UIR bands requires photons with UV (or short optical) wavelengths. The most prominent known exceptions to this general rule are the 21μm sources (Kwok et al. 1989; Justtanont et al. 1996), which are all G or F stars with relatively soft radiation fields. In these objects the emission is dominated by very broad plateau features, instead of the narrow features seen in PN, so that the difference in the nature of the radiation field has a major effect on the characteristics of the IR spectra. In the case of AFGL2688, we might expect further differences, because the radiation is effectively even softer. Although the central star appears to have a spectral type of F, the dust shell is remarkably optically thick. We adopted in Sect. 5 an optical depth at 10μm of order 2.0 in our line of sight. This yields an optical depth at 0.4μm (a wavelength short enough to excite UIR bands) of 50, so that photons with wavelengths short enough to excite the UIR bands can penetrate only a very tiny distance into the supershell before being absorbed. Under these circumstances, we cannot expect to see strong UIR band emission whether the carriers are present or not.

In practise, however, the 3.3μm UIR band has been observed in the spectrum of AFGL2688 (Geballe et al. 1992). The flux at the peak of the band is roughly comparable to that of the underlying continuum. The continuum at 11.3μm is about a thousand times brighter than that at 3.3μm (Fig. 14). For a wide range of sources, Jourdain de Muizon, d'Hendecourt & Geballe (1990) found that the ratio of the intensities of the 11.3 and 3.3μm UIR bands was of order ten. Adopting this value, we would expect any 11.3μm UIR band in the AFGL2688 spectrum to have a flux of only about 1% of the underlying continuum – in other words, we would probably not detect it even if it is present.

However, it is worth considering further the nature of the 3.3μm emission. The optical depth at 3.3μm is, on the basis of our radiative transfer model, about 6. This means that we should only be able to see 3.3μm emission from material close to the outer edge of the supershell. However, as pointed out above, the optical depth at the wavelength of the exciting photons is of order 50, so that material close enough to the surface of the supershell to be visible to us cannot then be excited by radiation from the central star. It would seem that the only ways we can observe 3.3μm emission from AFGL2688 are if the emitting material is close to the inner edge of the supershell, and the radiation is scattered towards us out of the reflection lobes, or if the emitting material is itself inside the lobes. In the former case we would predict that the 3.3μm feature in AFGL2688 should be strongly polarised. There appear to be roughly comparable fluxes of thermally emitted and scattered radiation at 3.3μm. If the 3.3μm feature is primarily scattered, then because the scattering cross-section drops rapidly with increasing wavelength the 11.3μm feature should be very much weaker than the 3.3μm feature. Temperature maps made with the various combinations of the 8.8, 10.0 and 11.5μm images do not differ significantly from one another, confirming that even in the outer parts of the mid-IR images, where direct emission from the UIR band carriers might be important, the UIR bands (which should contribute to the 8.8 and 11.5μm images, but not to the 10.0μm image) are very weak. This tends to favour the suggestion that the 3.3μm UIR band is principally emission from the inner edge of the torus scattered out of the reflection lobes, but the evidence is far from conclusive. Polarization images in the 3.3μm UIR band and in the nearby continuum will be enormously valuable in constraining the structure of this nebula and the nature and distribution of solid state material in it.

7. Conclusions

We have shown that the standard model of AFGL2688 cannot satisfactorily explain a large fraction of the observational data. Instead we have proposed a major revision of the model, which still involves a dense, dusty torus generating a bipolar flow, but with very different geometry to that employed in the standard model. We have shown how this can explain all the new observations we have presented, as well as all the existing

data. Using a full radiative transfer code in axial symmetry we have constructed a model which provides an excellent fit to the SED and a reasonable fit to most of the images from the optical into the far-IR/mm regions. In our model the progenitor star must have left the AGB about two hundred years ago with a dramatic burst of equatorially concentrated mass-loss which ejected about $0.7M_{\odot}$ of its envelope over a period of a few hundred years. The results imply that the star must have had a fairly large initial mass, near the upper end of the AGB mass range. We suggest that the Cygnus Egg Nebula may develop into a high excitation PN with similar morphology to NGC7027.

Acknowledgements. This work was supported in part (CJS & JRB) under the auspices of the U.S. Department of Energy by Lawrence Livermore National Laboratory under Contract No. W-7405-ENG-48. We are grateful to many members of the UKIRT and IRTF staffs for assistance with the observations. In particular we are indebted to Dolores Walther and Colin Aspin for invaluable assistance with the IRCAM data reduction. We are grateful to the Laboratory for Experimental Astrophysics and the Institute of Geophysics & Planetary Physics at LLNL, who supported the operation of the 10μm camera, and to Hughes Aircraft who supplied the mid-IR array used in the camera. Many thanks are due to Drs. Issei Yamamura and Shuji Deguchi, who provided us with their ^{13}CO images prior to publication, thereby giving us a great deal more confidence that our ideas were reasonable. Thanks are also due to Icko Iben for very valuable discussions, to Jack Fix for helping to make Sect. 5 possible, and to Pierre Cox for great encouragement at an important point in this work. Finally, thanks to Dr. Olsen and the boys in the lab' for introducing us to decaffeinated coffee.

References

Arens, J. F., Jernigan, J. G., Ball, J. R., Peck, M. C., Gaalema, S., Lacy, J. H., 1987a, in Infrared Astronomy with Arrays, eds C. G. Wynn-Williams & E. Becklin, University of Hawaii, Honolulu, p. 28

Arens, J. F., Jernigan, J. G., Peck, M. C., Dobson, C. A., Kilk, E., Lacy, J. H., Gaalema, S., 1987b, Appl. Opt., **26**, 3846.

Aspin, C., Schwarz, H. E., Smith, M. G., Corradi, R. L. M., Mountain, C. M., Wright, G. S., Ramsay, S. K., Robertson, D., Beard, S. M., Pickup, D. A., Geballe, T. R., Bridger, A., Laird, D., Montgomery, D., Glendinning, R., Pentland, G., Griffin, J. L., Aycock, J., 1993, A&A 278, 255

Balick, B., 1987, AJ 94, 671

Balick, B., Rugers, M., Terzian, Y., Chengular, J. N., 1993a, ApJ 411, 778

Balick, B., Perinotto, M., Maccioni, A., Terzian, Y., Hajian, A., 1993b, ApJ 424, 800

Ball, J. R., Arens, J. F., Jernigan, J. G., Keto, E., Meixner, M. M., 1992, ApJ 389, 616

Barvainis, R., McIntosh, G., Predmore, C. R., 1987, Nature, 329, 613

Beckwith, S., Beck, S. C., Gatley, I., 1984, ApJ 280, 648

Bieging, J. H., Rieu, N-Q., 1988, ApJ 324, 516

Castor, J. I., Lutz, H. H., Seaton, M. J., MNRAS 194, 547

Cernicharo, J., Guélin, M., Martin-Pintado, J., Peñalver, J., Mauersberger, R., 1989, A&A 222, L1

Cohen, M., Kuhi, L. V., 1977, ApJ 213, 79

Cohen, R. J., 1989, Rep. Prog. Phys., 52, 881

Collison, A. J., Fix, J. D., 1991, ApJ 368, 545

Corradi, R. L. M., Schwarz, H. E., 1993, A&A 278, 247

Cox, P., 1993, in Astronomical Infrared Spectroscopy: Future Observational Directions, ed. S. Kwok, ASP Conf. Series 41, p. 163

Crampton, D., Cowley, A. P., Humphreys, R. M., 1975, ApJ 198, L135

Deutsch, L. K., 1990, Ph.D. Thesis, Harvard University

Geballe, T. R., Tielens, A. G. G. M., Kwok, S., Hrivnak, B. J., 1992, ApJ 387, L89

Graham, J. R., Serabyn, E., Herbst, T., Beckwith, S., Matthews, K., Neugebauer, G., Soifer, B. T., Wilson, T. D., 1993, AJ 105, 250

Granato, G. L., Danese, L., 1994, MNRAS 268, 235

Griffin, I. P., 1990, MNRAS 247, 591

Heiligman, G. M., Berge, G. L., Claussen, M. J., Leighton, R. B., Lo, K. Y., Masson, C. R., Moffett, A. T., Phillips, T. G., Sargent, A. I., Scott, S. L., Scoville, N. Z., Wannier, P. G., Woody, D. P., 1986, ApJ 308, 306

Hoare, M.G. 1990, MNRAS 244, 193

Hora, J. L., Latter, W. B., 1994, ApJ 437, 281

Hora, J. L., Deutsch, L. K., Hoffmann, W. F., Fazio, G. G., 1995, in Circumstellar Matter 1994, ed. G. D. Watt & P. M. Williams, Kluwer, Dordrecht, p. 361

Hu, J. Y., Slijkhuis, S., Rieu, N-Q, de Jong, T., 1993, A&A 273, 185

Iben, I., 1983, ApJ 260, 821

Jaye, D., Tresch Fienberg, R., Fazio, G. G., Gezari, D. Y., Hoffmann, W. F., Lamb, G. M., Shu, P. K., McCreight, C. R., 1989, AJ 97, 809

Jourdain de Muizon, M., d'Hendecourt, L. B., Geballe, T. R.., 1990, A&A 227, 526

Jura, M., Kroto, H. 1990, ApJ 352, 222

Justtanont, K., Skinner, C. J., Tielens, A. G. G. M., 1994, ApJ 435, 852

Justtanont, K., Barlow, M. J., Skinner, C. J., Roche, P. F., Aitken, D. K., Smith, C. H., 1996, A&A 309, 612

Justtanont, K., Tielens, A. G. G. M., Skinner, C. J., Haas, M. R., 1997, ApJ 476, 319

Keto, E., Ball, J. R., Arens, J. F., Jernigan, J. G., Meixner, M., 1992, Int'l. J. of Infrared and Millimeter Waves 13, 1709

Kleinmann, S. G., Sargent, D. G., Moseley, S. H., Harper, D. A., Loewenstein, R. F., Telesco, C. M., Thronson, H. A., 1978, A&A 65, 139

Knapp, G. R., Phillips, T. G., Leighton, R. B., Lo, K. Y., Wannier, P. G., Wootten, H. A., Huggins, P. J., 1982, ApJ 252, 616

Knapp, G. R., Morris, M., 1985, ApJ 292, 640

Knapp, G. R., Bowers, P. F., Young, K., Phillips, T. G., 1994, ApJ 429, L33

Kwok, S., Volk, K. M., Hrivnak, B. J., 1989, ApJ 345, L51

Latter, W., B., Maloney, P. R., Kelly, D. M., Black, J. H., Rieke, G. H., Rieke, M. J., 1992, ApJ 389, 347

Latter, W. B., Hora, J. L., Kelly, D. M., Deutsch, L. K., Maloney, P. R., 1993, AJ 106, 260

Lightfoot, J. F., Glencross, W. M., 1986, MNRAS 221, 993

McLean, I. S., Chuter, T. C., McCaughrean, M. J., Rayner, J. T., 1986, in Instrumentation in Astronomy VI, SPIE 627, 430, ed. D. L. Crawford

Meixner, M., 1993, Ph.D. Thesis, University of California Berkeley.

Meixner, M. M., Skinner, C. J., Temi, P., Rank, D., Bregman, J., Ball, J. R., Keto, E., Arens, J. F., Jernigan, J. G., 1993, ApJ 411, 266

Meixner, M. M., Skinner, C. J., Graham, J. R., Keto, E., Jernigan, J. G., Arens, J. F., 1997, ApJ 482, 897

Morris, M., 1980, ApJ 236, 823

Morris, M., Guilloteau, S., Lucas, R., Omont, A., 1987, ApJ 321, 888

Neri, R., Garcia-Burillo, S., Guelin, M., Cernicharo, J., Guilloteau, J., Lucas, R. 1993, A&A 262, 544

Ney, E. P., Merrill, K. M., Becklin, E. E., Neugebauer, G., Wynn-Williams, C. G., 1975, ApJ 198, L129

Peimbert, M., 1978, in IAU Symposium No. 76: Planetary Nebulae, ed. Y. Terzian, Reidel, Dordrecht, p. 215
Piña, R., 1994, Ph.D. Thesis, University of California San Diego
Reid, M. J., Moran, J. M., Leach, R. W., Ball, J. A., Johnston, K. J., Spencer, J. H., Swenson, G. W., 1979, ApJ 239, 89
Schmidt, G. D., Cohen, M., 1981, ApJ 246, 444
Shibata, K. M., Tamura, S., Deguchi, S., Hirano, N., Kameya, O., Kasuga, T., 1989, ApJ 345, L55
Skinner, C. J., Meixner, M. M., Hawkins, G., Keto, E., Jernigan, J. G., Arens, J. F., 1994, ApJ 423, L135
Smith, M. G., Geballe, T. R., Sandell, G., Aspin, C., 1990, in Submillimetre Astronomy, eds G. D. Watt & A. S. Webster, Kluwer, Dordrecht, p. 29
Thronson, H. A., 1982, AJ 87, 1207
Truong-Bach, Morris, D., Rieu, N-Q., Deguchi, S., 1990, A&A 230, 431
Vassiliadis, E., & Wood, P.R., 1994, ApJS 92, 125
Wood, P.R., & Faulkner, D.J., 1986, ApJ 307, 659
Wood, P.R., & Vassiladis, E., 1993, in IAU Symp. No. 155: Planetary Nebulae, ed. Weinberger, R., & Acker A., Kluwer, Dordrecht, p. 291
Yamamura, I., Onaka, T., Kamijo, F., Deguchi, S., Ukita, N., 1995, ApJ 439, L13
Young, K., Serabyn, G., Phillips, T. G., Knapp, G. R., Güsten, R., Schulz, A., 1992, ApJ 385, 265
Yusef-Zadeh, F., Morris, M., White, R. L., 1984, ApJ 278, 186

This article was processed by the author using Springer-Verlag LaTeX A&A style file *L-AA* version 3.